**TECHNISCHE
UNIVERSITÄT
WIEN**
Vienna University of Technology

Diplomarbeit

In Situ Comparison Between Direct and Magnetization Reel-to-Reel Critical Current Measurements in REBCO Coated Conductors

Ausgeführt am
Atominstitut, Technische Universität Wien
und am
**National High Magnetic Field Laboratory,
Tallahassee, Florida, USA**
unter der Anleitung von

Univ. Prof. Dr. Dr.h.c. Harald W. Weber
und
Dr. Jan J. Jaroszynski,
Prof. Dr. David C. Larbalestier

durch

Alexander Stangl
Matrikelnummer: 0825699
Kleine Pfarrgasse 7/17
1020 Wien

28. November 2013

Abstract

High temperature superconductors, made from $REBa_2Cu_3O_{7-x}$ (RE = rare earth element) in the form of coated conductors are playing an increasing role in the fabrication of magnets and the development of high current and high field applications. For these purposes high critical current densities J_c and good magnetic properties homogeneous over the full length (hundreds of meters) of the tape are necessary.

This thesis presents results of in situ magnetization and I_c reel-to-reel measurements in several tapes of REBCO coated conductors from Superpower Inc. with lengths of more than $100\,m$. Reel to reel measurements enable continuous critical current $I_c(x, B, \theta)$ evaluations of superconducting tapes for commercially available lengths of superconducting tape with very high resolution. Further, an array of Hall probes was installed for magnetization measurements and contact free observation of the current flow, which provide a reliable and very fast, but non-calibration free opportunity for the analysis of long tapes. We made detailed comparisons of those two methods. Our results confirm the validity of the magnetization method to find inhomogeneities. The possibility of identifying defects in tapes is crucial for the construction of magnets, since a single defect degrades the performance of the whole magnet.

Up to now these non-destructive measurements were made at liquid nitrogen temperature. We developed a measurement setup for reel-to-reel Hall probe measurements at liquid helium temperature. Such measurements are unique at present. This temperature range is interesting, because the construction of all-superconducting magnets for generating fields above $30\,T$ requires cooling to $4.2\,K$. While coated conductors are widely characterized at $77\,K$, the flux pinning mechanisms are poorly known at temperatures below $T_c/2$. These mechanisms may be very different at high and low temperatures. Because of the strong reduction of thermal fluctuation effects weaker flux pins are becoming more important at low temperatures.

Zusammenfassung

$REBa_2Cu_3O_{7-x}$ (RE = Seltene Erdelemente) Hochtemperatursupraleiter in Form von sogenannten coated conductors spielen eine immer wichtiger werdende Rolle beim Bau von starken Magneten und der Entwicklung von Strombegrenzungsanlagen und anderen Anwendungen in der Energietechnik. Für diese Zwecke sind sehr hohe und homogene kritische Stromdichten J_c und gute magnetische Eigenschaften über die gesamte Länge von kilometerlangen Leitern notwendig.

Diese Arbeit präsentiert Ergebnisse von in situ Magnetisierungs- und Transportstrommessungen von verschiedenen REBCO coated conductors der Firma SuperPower Inc. mit Längen bis zu 120 m. Der Leiter wird von einer Abwickelspule auf eine Aufwickelspule gewickelt (reel-to-reel). Zwischen den Spulen befinden sich Messkontakte und Sensoren, an denen der Leiter vorbei transportiert wird. Dieser Messaufbau ermöglicht das kontinuierliche Messen des kritischen Stromes $I_c(x, B, \theta)$ von kommerziellen supraleitenden Bändern mit einer sehr hohen räumlichen Auflösung. Die Erweiterung des Messaufbaues mit einem Array von Hallsonden ermöglicht eine kontakt- und zerstörungsfreie und sehr schnelle Analyse von langen Bandleitern. Der Vergleich von Transportstrom- und Magnetisierungsmessungen bestätigt die Gültigkeit der in mehreren Laboratorien weltweit praktizierten Magnetisierungsmethode zur Evaluierung des kritischen Stromes. Die Untersuchung von REBCO Leitern auf mögliche Defekte ist von großer Bedeutung für deren Einsatz in Magneten und anderen Anwendungen, da ein einziger Defekt die gesamte Charakteristik des Magneten stark beeinträchtigt.

Bislang werden Bandleiter in voller Länge nur bei 77 K untersucht. Im Rahmen dieser Arbeit wurde ein Aufbau für reel-to-reel Magnetisierungsmessungen bei 4.2 K entwickelt. Die Möglichkeit kontinuierliche Messungen in flüssigem Helium durchzuführen ist derzeit weltweit einzigartig. Dieser Temperaturbereich ist insofern von Bedeutung, da Systeme, die hohe kritische Stromdichten und hohe kritische Felder voraussetzen, bei 4.2 K operieren. Die Analyse von Bandleitern bei 77 K ist a priori nicht hinreichend, da sich durch die starke Abnahme von thermischen Fluktuationen im Supraleiter das Pinningverhalten ändert und schwächere Pinningzentren wichtiger werden.

Acknowledgments

This thesis was written at the Applied Superconductivity Center of the National High Magnetic Field Laboratory in Tallahassee, Florida USA.

I would like to thank my supervisor Harald W. Weber for his cross-border engagement leading to this opportunity for my stay at the NHMFL. I highly appreciate his encouragement and interest in my research work from my first day at the Atominstitut in Vienna.

I also want to express my gratitude to David C. Larbalestier for giving me the exciting chance of working in his group and his constant scientific input during my stay.

Further I wish to thank Jan J. Jaroszynski for our long discussions and his continuous helpful tips and advise and especially for his individual support settling down in Tallahassee as well as John Sinclair for his introduction to YatesStar and his effort to help solving problems in all kinds of situations. My gratitude also goes to Michael Santos and Van Griffin for their technical assistance and Xinbo Hu for his assistance with the measurements.

Without Connie Linville and Charlotte Hall I would not have been able to find a way through bureaucracy. Thank you for being family for all of us aliens. Furthermore I want to thank all ASC graduate students and members and my colleagues at the ATI in Vienna for their warm welcome.

Finally I would like to express my deep gratitude to my parents Monika and Gerhard for their vast support for my path wherever I'm going.

Contents

1 Introduction and Motivation

The present work is concerned with the analysis of long superconducting $YBa_2Cu_3O_{7-x}$ tapes. The motivation of this work is the use of these high temperature superconductors (HTS) in several applications, especially the 32 T all-superconducting magnet project at the National High Magnetic Field Laboratory (NHMFL). For these purposes high critical current densities J_c and good magnetic properties homogeneous over long lengths are necessary.

In this work we upgraded an apparatus, YatesStar [1–3], for simultaneous magnetization and I_c reel-to-reel measurements of REBCO tapes with lengths of more than 100 m at liquid nitrogen temperature and developed the possibility of - at present - unique continuous magnetization measurements at liquid helium temperature.

Although superconductivity is known for more than 100 years and alloys with transition temperatures above the boiling temperature of liquid nitrogen were discovered 25 years ago, superconductivity is still in the interest of research groups all over the world to understand the fundamental physics of especially type II superconductors and to use the benefits and attractive perspectives for applications. At the moment a 32 T all-superconducting magnet is developed at the NHMFL, by combining outer coils made of low temperature superconductors (LTS) and inner coils of high temperature superconductors. The use of YBCO coated conductors (CC) as HTS material provides an increase in central field and a large reduction of operation costs compared to resistive magnets [4]: a normal resistive (Bitter) magnet at the NHMFL at 15 T consumes 6.8 MW, a superconducting magnet with the same field less than 1 kW. Further, superconducting magnets have much better homogeneity and a more constant field over time, which is very important to magnetic resonance measurements and such magnets can be built more compactly due to the capacity of carrying higher currents.

There is one commercial quality inspection tool for superconducting tapes, Tapestar from THEVA GmbH, and several scientific projects of long tape analysis, all based on magnetization measurements with Hall probes at 77 K [5–8]. The innovation of our work is the comparison of transport current I_c measurements and magnetization measurements over the full length of superconducting tapes at 77 K and the latter as well at 4.2 K. Transport current measurements need several contacts (at least two voltage and two current contacts) which could damage the tape by friction or too high currents (currents well above I_c) and continuous measurements are not possible, since the current must be ramped to determine the critical current defined by a certain electric field criterion. During this process, which has a finite duration, the tape cannot be moved. To avoid noise produced by the motion of the tape, current sweeps, local changes of the field, thermal heating and others, a pause before each local I_c measurement is reasonable, which extends the time of the analysis. In comparison, Hall probe measurements are fast, contact-free

and therefore non-destructive with high spatial resolution. On the other hand they are susceptible to various influences and need no calibration. The possibility to use both methods, or rather in situ one after the other, allows us to test and confirm the validity of magnetization measurements to assess the local critical currents and find influence factors to further improve the tape analysis using Hall probes. Since magnet bores in cryostats are limited to a few centimeters, a very compact measuring setup is essential for low temperature measurements. Transport measurements in this temperature range would need thick current leads to carry high currents without Joule heating. These requirements are hardly compatible with the given space in the bore. Therefore Hall probe measurements are a promising candidate for this very low temperature range.

Previously it was shown for short samples [9], that efforts to optimize the conductor production for high temperature applications lead to an increasing I_c at 77 K, but reduce at the same time in-field properties at liquid helium temperature. Intensive studies of pinning mechanisms, especially introduced by $BaZrO_3$ nanorods at the Applied Superconductivity Center [9–11] have shown, that there is no a priori known correlation between 77 K and 4.2 K. There might be different flux pinning mechanisms due to smaller vortex core sizes and the reduction of thermal fluctuations at low temperatures, which allow weaker pins to become more important. These results make the characterization of CCs at low temperatures essential for their use in low temperature applications.

Summing up, the aim of this work is to develop fast and non-destructive magnetization measurements, prove their validity in comparison with local transport measurements over long lengths at liquid nitrogen temperature and - based on these results and the experiences gained - build a prototype for reel-to-reel magnetization measurements at 4.2 K.

1.1 Superconductivity

Superconductivity is a state with extraordinary electrical properties which occurs at low temperatures. Superconductors lose electric resistance below a certain material-dependent temperature, the critical temperature T_c. This property is limited by a critical current density J_c, an external critical field and as well the temperature T_c. Zero resistance is essential but not sufficient to make superconductivity a thermodynamic phase. Only in combination with the ejection of weak external magnetic fields are these requirements fullfilled. This second very important characteristic of superconductivity is called the Meißner effect [12]. The limiting field for type-I SC is the thermodynamic critical field B_c which is defined by the difference in the Gibbs free energy G of the normal and superconducting state, the condensation energy E_c in zero field

$$E_c = G_n(0, T) - G_s(0, T) = \frac{\mu_0 H_c^2(T)}{2} V \sim \Delta^2, \tag{1.1}$$

with V as volume of the sample, μ_0 as the vacuum permeability and 2Δ as the energy gap. This energy difference is due to the condensation of pairs of electrons with opposite wave vectors and spins into Cooper pairs caused by a small attraction between electrons

8

and phonons. The expansion of a Cooper pair is described by the intrinsic coherence length $\xi_0 \sim v_F/\Delta(0)$, with v_F as the electron velocity at the Fermi surface. ξ_0 is characteristic of a pure superconductor, thus called BCS coherence length. The condensation energy is proportional to the energy gap. Due to the pairing mechanism former fermion particles behave like bosons and those electron pairs are not subject to the Pauli exclusion principle, which states that each quantum state is occupied by a single particle only. Therefore with transition into the superconducting phase electrons form Cooper pairs, which can occupy lower energy levels and a superconducting energy gap opens in the energy spectrum. Normal resistivity is caused by the scattering of charge carriers by impurities. In a superconductor interactions with the lattice are impossible, because there are no quantum states available within the range of the interaction energy. The absence of scattering processes results in zero resistivity.

1.2 Superconductors in External Magnetic Fields

There are several classifications for superconductivity which occurs in certain materials. Superconductors can be classified as type-I and type-II SC by their behavior in external magnetic fields, which is determined by the surface energy σ_{ns} at the boundary between normal and superconducting phases. Those two types can be distinguished by the material-dependent Ginzburg-Landau parameter κ

$$\kappa = \frac{\lambda}{\xi_{\mathrm{GL}}}, \tag{1.2}$$

with λ as length of the spatial change of the magnetic field (penetration depth) and ξ_{GL} as the Ginzburg-Landau coherence length, a scale over which the Cooper pair density n_{C} can vary [13]. κ is smaller than $1/\sqrt{2}$ for type-I superconductors and greater than $1/\sqrt{2}$ for type-II superconductors. The theoretically temperature independent parameter κ is sufficient to describe a superconductor within the Ginzburg-Landau theory [14]. κ ranges from ~ 0.01 for pure metals to 500 for high temperature superconductors.

At an interface of a normal and superconducting phase $n_{\mathrm{C}}(T)$ must be zero but cannot jump abruptly from the value $n_{\mathrm{C}}(T)$ in the interior of the superconductor to zero at the boundary. If the critical magnetic field B_{c} is applied at the N-S-interface, the condensation energy $E_{\mathrm{c}} < 0$ and the exclusion energy $E_b > 0$ (the energy required to exclude the magnetic field) inside the superconductor are equal by absolute value. The exclusion energy and the condensation energy compete near the interface.

1.2.1 Type-I Superconductivity

If $\lambda \ll \xi_{\mathrm{GL}}$ ($\kappa \ll 1$) E_{b} reaches rapidly its full value, while E_{c} grows slowly. Thus, the energy difference $\Delta E = E_{\mathrm{c}} + E_{\mathrm{b}}$ and the interfacial energy σ_{ns} are positive. In equilibrium the S-N-boundary reaches a minimum [15] and the superconductor expels weak magnetic fields (Meißner effect, section 1.1). If the external field exceeds the critical field $\mu_0 H_{\mathrm{c}}$ superconductivity vanishes. Pure element superconductors are mostly type-I.

1.2.2 Type-II Superconductivity

Otherwise, if $\lambda \gg \xi_{\mathrm{GL}}$ ($\kappa \gg 1$) the negative condensation energy exceeds the exclusion energy: $\Delta E < 0$ and also $\sigma_{\mathrm{ns}} < 0$. The ratio area/volume (of the interface to the sample volume) gets bigger until it reaches a quantum limit. This state is called Shubnikov phase (mixed state) and defines type-II superconductors. With the change of the sign of the boundary energy the properties of the superconductor change drastically. Quantized magnetic flux vortices penetrate the superconductor, which was predicted by Abrikosov [16] in 1957.

Type-II superconductors have two critical fields, the lower critical field $B_{\mathrm{c}_1} < B_{\mathrm{c}}$ and the upper critical field $B_{\mathrm{c}_2} \gg B_{\mathrm{c}}$. If the external field B_{ext} is below B_{c_1}, the superconductor is in the Meißner phase and shows perfect diamagnetism. Increasing the applied field to $B_{\mathrm{ext}} > B_{\mathrm{c}_1}$, the field cannot be expelled completely and magnetic flux lines penetrate the superconductor. One single flux line carries a quantum of magnetic flux: a flux quantum $\Phi_0 = \frac{h}{2e} = 2.07 \cdot 10^{-15}\,\mathrm{Wb}$. The exclusion energy, which increases the Gibbs free energy of the superconducting state in a magnetic field, is reduced by the penetration of the magnetic field. Therefore, larger external fields are required to raise the free enthalpy of the superconducting state until it becomes the same as that of the normal state [13]. If $\lambda \gg \xi_{\mathrm{GL}}$ we can neglect the reduction in condensation energy due to the field penetration. The system is in Shubnikov phase until B_{ext} exceeds the second critical magnetic field B_{c_2}, where it looses superconductivity. The second London equation (developed by F. and H. London as extension of the Maxwell equation to describe the electromagnetic properties of a superconductor)

$$\mathrm{curl}(\Lambda \vec{j}_{\mathrm{s}}) = -\vec{B} \tag{1.3}$$

gives a relation between magnetic field $\vec{B}$ and supercurrent density $\vec{j}_{\mathrm{s}}$. Thus, a non-vanishing magnetic field always causes a supercurrent flowing inside the superconductor. The current circulates around the flux lines, modifies the magnetic field and effects thereby spatial variations of both the magnetic field and the supercurrent density.

1.3 High Temperature Superconductors HTS

The discovery of superconductivity in $\mathrm{Ba}_x\mathrm{La}_{5-x}\mathrm{Cu}_5\mathrm{O}_{5(3-y)}$ in 1986 by Bednorz and Müller [17] brought a renaissance for research in superconductivity. The first superconductor with a transition temperature above $77\,\mathrm{K}$ was announced in 1987: $\mathrm{YBa}_2\mathrm{Cu}_3\mathrm{O}_x$ at $92\,\mathrm{K}$ [18]. In the following years superconductivity was found in many compounds with T_{c}s far beyond $100\,\mathrm{K}$ [19] and above $150\,\mathrm{K}$ under high pressures [20, 21]. Several important discoveries over the last 100 years are shown in a timeline in figure 1.1. Whereas conventional superconductivity is based on the interaction between electrons and lattice vibrations and is described by BCS theory (Bardeen et al. [22]), there is no widely accepted theory of HTS to explain their physical properties. HTS was found in three different kinds of materials: cuprates, magnesium diboride (MgB_2) [23] and iron-based compounds [24, 25]. All known HTS are type-II superconductors.
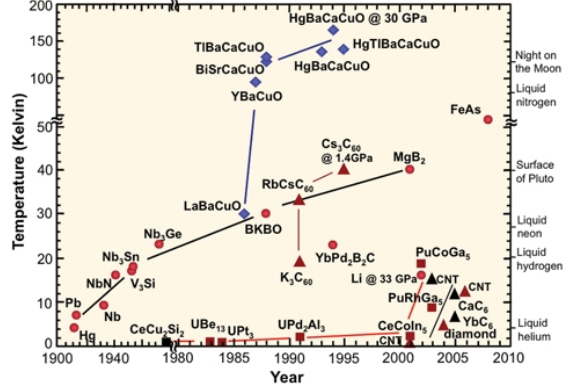
Figure 1.1: Timeline of discoveries of superconducting materials [26]

1.4 Bean's Critical State Model

As shown in section 1.2 there are two different kinds of superconductivity, determined by their behavior in external magnetic fields. Type-II superconductors generally show an irreversible magnetization if subjected to an applied field above B_{c_1}, because vortices become pinned by microstructural defects. After intensive studies of magnetization curves of "hard" superconductors Bean [27, 28] published his theory of the magnetization hysteresis of high-field superconductors. The following assumptions are valid only if there is a macroscopic gradient, which requires pinning (there are reversible type-II superconductors, which show no hysteresis). Under the premise that a limiting macroscopic superconducting current density exists, he assumed that fields below $\mu_0 H_{c_1}$ are screened by screening currents flowing only at the surface. Further fields $\mu_0 H$, $H_{c_1} < H < H_{c_2}$, are shielded by local currents flowing in layers to the full amount of the critical current density. Hence, the sample carries a maximum supercurrent. In his first approximation the current density is field independent ($J_c(B) = const.$). This treatment is appropriate as long as the applied field is much less than the critical field, especially since the difference $H_a - H^*$ is relevant. Kim et al. [29] introduced an inversely proportional relation for the field dependence of the current density. There are several relations in literature to describe J_c as a function of magnetic field in different regions of the field.

   The process of magnetization can be described by steps as shown in figure 1.2 for an ideal infinite cylinder with diameter D. Increasing the applied field from $H = 0$ (more precisely from $H = H_{c_1}$, but for type-II SC H_{c_1} is very small) to $H = H^*$ quantized magnetic flux penetrates the outer layers of the superconductor. Pinning centers establish a gradient of flux lines producing a local current. Since we assumed a constant current density of J_c, the decrease of the field may be linear, as predicted by Ampère's law. The penetration depth is therefore field dependent. At an applied field of $H = H^*$ the whole sample is penetrated by field and the current density is non-zero everywhere in the sample. Further increasing fields cannot be shielded more efficiently. In this simple model $H(r = 0) = H(r = \frac{D}{2}) - H^*$ describes the field in the center of the sample, if
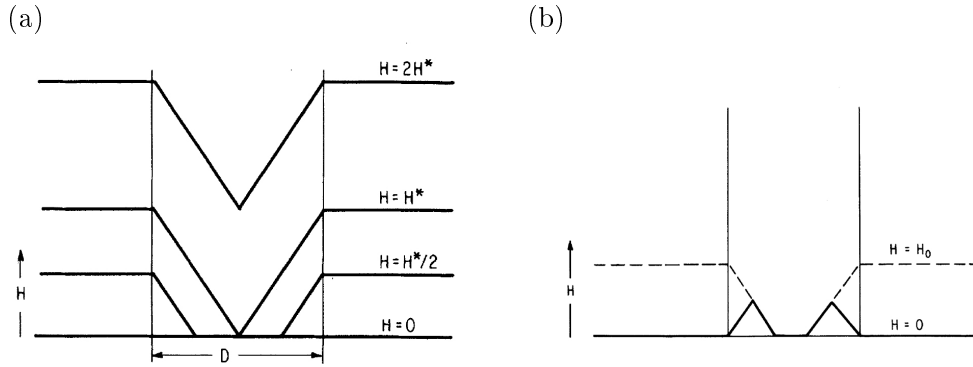
Figure 1.2: The local fields inside the superconductor for (a) increasing and (b) decreasing external fields described by the Bean model [28]

the applied field H exceeds H^*. Fig. 1.2 (b) shows the remanent magnetization after a field H_0 has been applied and removed. If the applied field $H \geq 2H^*$ the remanent magnetization in the center of the field reaches its maximum.

1.5 Yttrium Barium Copper Oxide Superconductors

Cuprates crystallize in a so called Perovskite structure and all cuprates like $YBa_2Cu_3O_{7-x}$ exhibit CuO_2 planes, which appear to be crucial for superconductivity in such systems [30]. Yttrium atoms can be replaced by other rare earth elements. A significant property of HTS and in particular for REBCO superconductors is the very small coherence length ξ_0 of about 1 nm which is caused by a small, or rather towards zero aiming mean free path. Therefore high angle grain boundaries strongly decrease the superconducting performance. This behavior is shown in figure 1.3. The crystal must grow epitaxially to achieve a high superconducting current density.

1.5.1 Crystal Structure of YBCO

Two crystalline structure occur in $YBa_2Cu_3O_{7-x}$, depending upon its oxygen content. If $x > 0.65$ the compound crystallizes in a tetragonal structure. In this case superconductivity is suppressed. A higher oxygen content leads to a superconducting orthorhombic structure with a maximum T_c at $x = 0.07$. The crystal structure is shown in figure 1.4. YBCO is structured in layers. The layer of yttrium atoms is situated between two CuO_2 layers. The oxygen content can only vary in between the CuO_2 layers and the CuO chains at the upper and lower edge of the unit cell (site O(1) and O(4) in fig. 1.4). The exchange of charge carriers between the CuO chains in b-direction of the crystal and the CuO_2 layer is very important for the occurrence of superconductivity. Table 1.1 gives information about the lattice parameters and the critical temperature for three superconduting phases in YBCO.
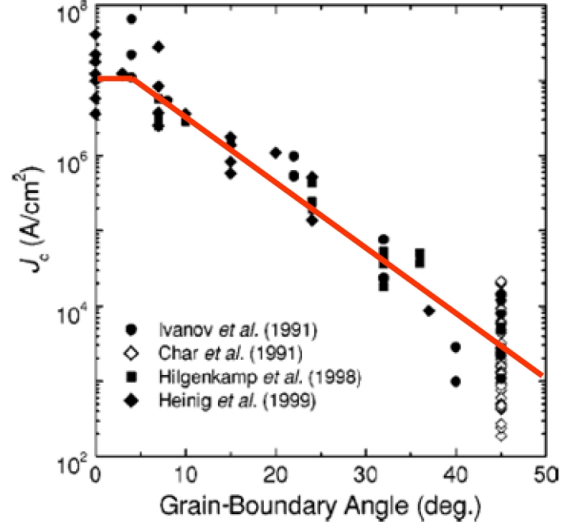
Figure 1.3: Linear decrease of the J_c with increasing grain-boundary angle in a logarithmic scale, i.e. an exponential dependence of J_c on the angle θ for angles $\gtrsim 5°$ [30, 31]

Superconductor	Crystal System	a (nm)	b (nm)	c (nm)	T_c (K)
$YBa_2Cu_3O_{7-x}$	Orthorhombic	0.382	0.389	1.168	92
$YBa_2Cu_4O_8$		0.384	0.384	2.720	80
$Y_2Ba_4Cu_7O_{14+x}$		0.383	0.389	5.059	40

Table 1.1: Lattice parameters and critical temperature for three superconducting phases of YBCO
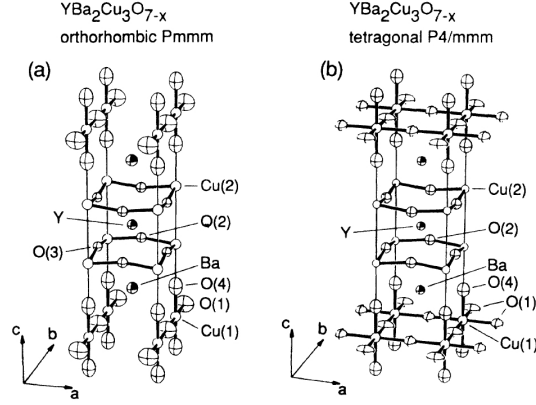
Figure 1.4: (a) Orthorhombic and (b) tetragonal structures of $YBa_2Cu_3O_{7-x}$. In the tetragonal structure (b) the different atom symbol for the O(1) site is used to indicate that this site is not fully occupied. O(2) and O(3) are always fully occupied. [30, 32]

1.5.2 Anisotropy

Due to the layered crystal structure of YBCO it is obvious that anisotropy occurs. A measure of the anisotropy is the parameter γ:

$$\gamma = \frac{\xi_{ab}}{\xi_c} = \frac{\lambda_c}{\lambda_{ab}} = \sqrt{\frac{m_c}{m_{ab}}} = \frac{H_{c2}^{ab}}{H_{c2}^{c}}, \tag{1.4}$$

with the coherence lengths ξ_{ab} and ξ_c and the London penetration depths λ_{ab} and λ_c in the ab-plane and c-axis. m_{ab} and m_c are the effective electron masses. For $YBa_2Cu_3O_{7-x}$ γ is close to 5 in overdoped YBCO like in coated conductors. The magnetic properties of cuprates are strongly anisotropic. There are huge differences between the upper critical field $B_{c2}(0\ K)$, if the field is parallel or normal to the CuO_2 layers. The effective electron mass is a measure of the mobility of charge carriers. A higher effective electron mass in the c-direction correlates with a higher resistivity perpendicular to the atom planes.

1.5.3 Flux Pinning of YBCO SC

Real crystals always contain defects and with such short ξ, there is a positional variation of the SC condensation energy comparable to ξ which sets up conditions for vortices to be pinned by such defects. In type-II superconductors flux lines penetrate the interior. The vortices in a SC free of defects are driven by an applied current due to the Lorentz force F_L due to a nonuniformly distributed flux line system [33]. This flux flow causes an electric field resulting in a decay of the current. Flux pinning is necessary to carry a bulk current density without losses. Vortex pinning is based on saving the loss of condensation energy E_c in the flux line cores at microstructural defects. The maximum pinning effect is reached by defects of a scale of $2\xi_{GL}$ with a similar density to the flux lines. Many

14

kinds of defects contribute to the pinning force F_p. There are natural imperfections, including oxygen vacancies, impurities and interstitial atoms (zero-dimensional), edge and screw dislocations of the crystal structure (one dimensional), two dimensional pinning centers like stacking faults and grain boundaries and volume defects. Further intrinsic pinning occurs in layered compounds, due to the suppressed superconductivity between CuO_2 planes. Artificial defects like nanoparticles, or defects introduced by irradiation can improve the in-field properties significantly. Often hole doping is necessary to enable electrical conductivity. A maximum T_c can be achieved by optimal doping [34]. Literature distinguishes between weak and strong pinning. For very weak pinning centers, a theoretical solution of the collective pinning model exists, resulting in a small critical current density [30, 35]. For high J_cs strong pinning centers are necessary, which even destroy the short range order of the vortex lattice, thus flux lines are individually and locally pinned [36]. Thermal fluctuations in high temperature superconductors degrade the pinning effectiveness [37]. The Ginzburg number Gi is a measure of the temperature interval susceptible for thermal fluctuations. For conventional superconductors Gi is about 10^{-8}, but 0.07 for YBCO [38]. This high number for YBCO is caused by a short coherence length and a high critical temperature. Therefore at high temperatures only strong pinning centers (1D, 2D and 3D) contribute to flux pinning. At the transition to low temperatures weak pins become more important, which could affect the critical current density and the anisotropy of cuprates.

The critical current is reached, if the pinning force is exceeded by the Lorentz force: $F_L = -F_p$. At a higher current, the flux lines are driven down the flux density gradient with energy dissipation. This state of motion is called flux flow. The superconductor remains in the superconductive phase, including quantized flux lines and Cooper pairs until J exceeds the depairing current density J_d. The depairing current density is reached when Cooper pairs break because their kinetic energy becomes equal to the superconducting energy gap 2Δ. A typical superconducting current-voltage characteristic is shown in figure 1.5.

It is now clear that the remanent magnetization, shown in figure 1.2 (b), is due to the irreversible penetration of flux vortices, which are pinned by defects. The pinning centers inhibit the flux from leaving the superconductor.
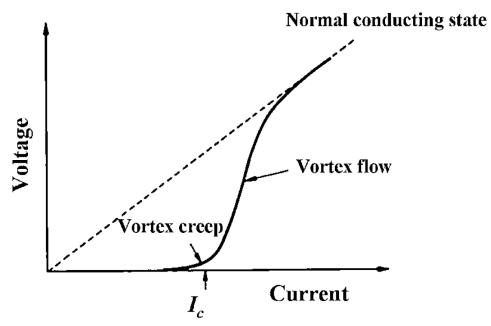
Figure 1.5: Current-voltage characteristic of a superconductor, where I_c is determined by the electric field criterion $1\,\mu\mathrm{Vcm}^{-1}$ [39]

2 Hall Probe Measurements

With the goal to show the possibilities of Hall probe (HP) measurements, we built several sensor heads with three or four Hall probes. Later we produced an array with seven HPs as well. We used transverse Hall generators 2101-100 from Lake Shore. The HPs are glued with GE varnish to the surface of a sample holder (16 pin DIP connector). Thus we are able to easily exchange the HP arrays. The HPs are connected in series to ensure the same driving current through all HPs and they are mounted with the same alignment.

2.1 Theory of Operation

The measurement of magnetic fields with Hall probes is based on the eponymous Hall Effect, discovered in 1879 by Hall [40]. Initiated by a statement in Maxwell's book about Electricity and Magnetism, he investigated the influence of a magnetic field on the current in a conductor. Predicted by the Lorentz force

$$\vec{F}_{\mathrm{L}} = q(\vec{E} + \vec{v} \times \vec{B}) \tag{2.1}$$

a point charge q with velocity $\vec{v}$ experiences a force in an external magnetic field $\vec{B}$. Due to a different sign, electrical positive and negative charges will be separated inside the current-carrying conductor. An excess charge on one side creates a transverse electric field which pushes the electrons in the opposite direction. At equilibrium this potential difference can be measured as shown in figure 2.1. Hall probe materials are mostly semiconductors from columns III and V of the periodic chart, which provide a high charge mobility. The Hall voltage is proportional to the magnetic field B and given by the relation

$$U_H = A_{\mathrm{H}} I B, \tag{2.2}$$

with the current I through the conductor and a material and thickness-dependent Hall coefficient.

2.2 Calibration of Hall Probes

According to equation 2.2 the transverse voltage across the Hall probe should vanish in zero field. In practice Hall probes show an offset. A calibration determines the offset and the Hall coefficient A_{H}.

To do so, we placed a Hall probe array in the center of a 1 T electromagnet and oriented it in the field. The applied field was measured by an installed and already calibrated
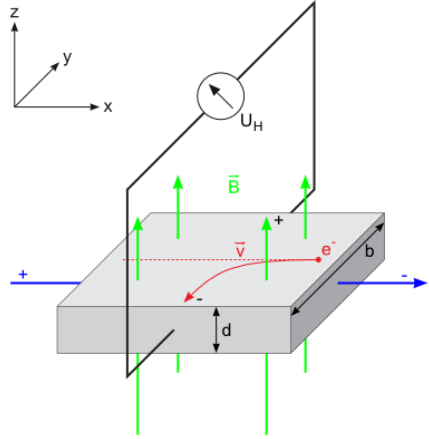
Figure 2.1: Schematic of operation of a Hall generator [41]

Hall probe. We used the AC and DC current modes to calibrate the Hall probes. In the AC mode the current was supplied by the internal function generator of a Stanford Research System 830 Lock-in amplifier, which was used to record the data as well. By changing the amplitude and measuring the voltage drop across a $1\,\mathrm{k\Omega}$ resistance we set the current to the desired value. In the DC mode a Lake Shore 120 current source provided the driving current. Later we changed to a Keithley Sourcemeter with a more stable current output. The Hall voltage was measured with a 2182a Nanovoltmeter from Keithley. In both modes we set the current through the HPs to $100\,\mathrm{\mu A}$ and increased the field by increasing the current in the electromagnet in several steps. At a given field we measured the voltage over a certain time and averaged the values. These mean values are shown in fig. 2.2 (a). For the linear regression we used the relation

$$U_\mathrm{H} = A_\mathrm{H}IB + U_0. \qquad (2.3)$$

Especially in low fields the offset U_0 is very important for the determination of the Hall coefficient A_H as shown in fig. 2.2 (b). If the voltage is non-vanishing, U_H/B goes to plus or minus infinity. A good correction leads to a satisfying linearity for the Hall coefficient up to $400\,\mathrm{mT}$, which is sufficient for our initial measurements. A_H results in $228\,\mathrm{VA^{-1}T^{-1}}$. With a control current of $100\,\mathrm{\mu A}$ the magnetic sensitivity is $22.8\,\mathrm{\mu V/mT}$. This high sensitivity allows us to measure tenths to hundredths of a millitesla.

In figure 2.3 two Hall probe arrays are shown. Fig. 2.3 (a) is the first produced sensor head. It consists of four Hall probes and was used for calibration measurements. The current contacts are connected serially. The sensor head is fixed on a 16 pin sample holder with pairs of twisted wires for the voltage and current contacts. The array in figure 2.3 (b) was used for magnetization measurements. The Hall probes are glued as closely as possible. The length of each HP is $1.5\,\mathrm{mm}$. The active area ($130\,\mathrm{\mu m}$, square) of the Hall probe is in the center of the sensor. Therefore, with three Hall probes as shown, a width of $\approx 3\,\mathrm{mm}$ is covered.

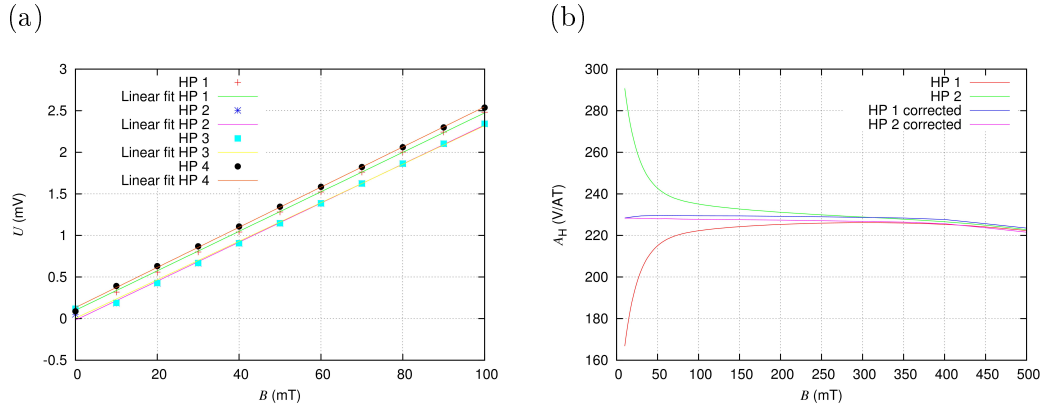(a)   (b)

Figure 2.2: Hall probe calibration (DC mode): (a) linear regression to determine the offset and (b) plot of the Hall coefficient A_H with and without offset correction

For more detailed observations a higher Hall probe density is necessary. An arrangement of seven Hall probes, each shifted by a third of its length relative to the vertical position of the previous array allows us to measure with a higher spatial resolution and to evaluate critical parameters. This array was fabricated by the electronic shop of the NHMFL. A draft and the produced sensor are shown in figure 2.4 (a & b). The tape is moving in x direction. There are three lines of HPs. The distances in x direction between the edges of the Hall probes between line 1 and line 2 and line 2 and line 3 are 1.5 mm, respectively. This distance can be neglected for measurements of long tapes and the comparison over the full length. At high resolution in x direction and small inspection lengths this distance must be taken into account. In the evaluation of I_c (section 3.3.4) all HPs are assumed to be on one straight line. The first line (HPs 1, 2) is shifted by 1.6 mm in minus z direction and the third line (HPs 6, 7) by 0.8 mm from the left edge of the second line (HPs 3, 4, 5). The distance between the Hall generators in one line is 0.3 mm, respectively. Therefore a width of 3.6 mm is covered by seven HPs and the resolution in z direction (direction of the tape width) is 0.6 mm. In the direction of tape movement the resolution is limited by the reading speed of the voltmeters, but can be increased by decreasing the tape velocity. The Hall probes 1, 4 and 7 are rotated by 180° to have the same current direction in each Hall generator with minimized length of the current contacts between the sensors.

2.3 Magnetoscan

The magnetoscan is a measurement technique to achieve a high resolution 2 d map of the trapped field in a high temperature superconducting sample [42, 43]. Therefore a permanent magnet is moved across the surface to induce shielding currents in the sample. This technique was developed and the magnetoscan measurements were performed at the Atominstitut in Vienna. A schematic is shown in figure 2.5. As shown, the sample and the Hall probe, which is fixed on a steel tube, are situated in an open dewar filled with liquid nitrogen. The Hall probe is moved by a stepper motor with a minimal increment

19

(a)   (b)
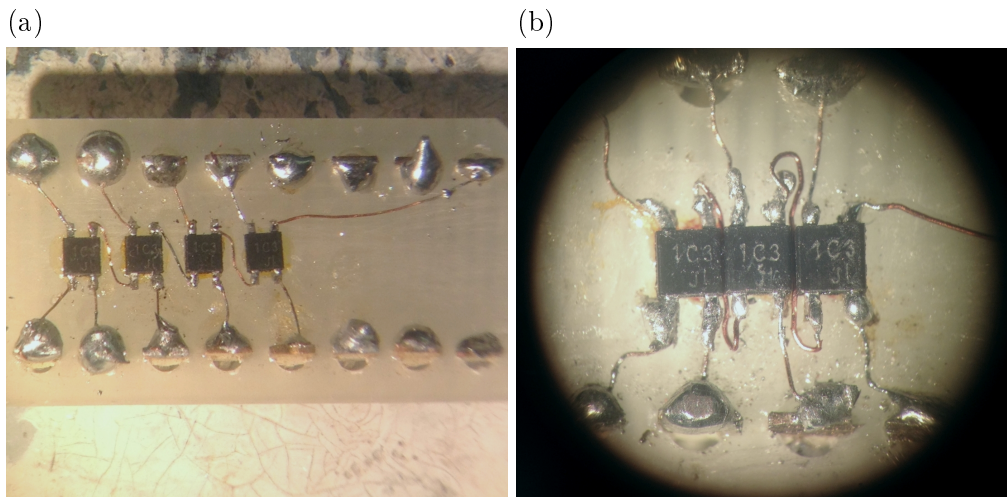
Figure 2.3: Hall probe sensor heads with (a) four Hall probes, used for calibration mea-
surements and (b) three Hall probes mounted closely to each other for tape
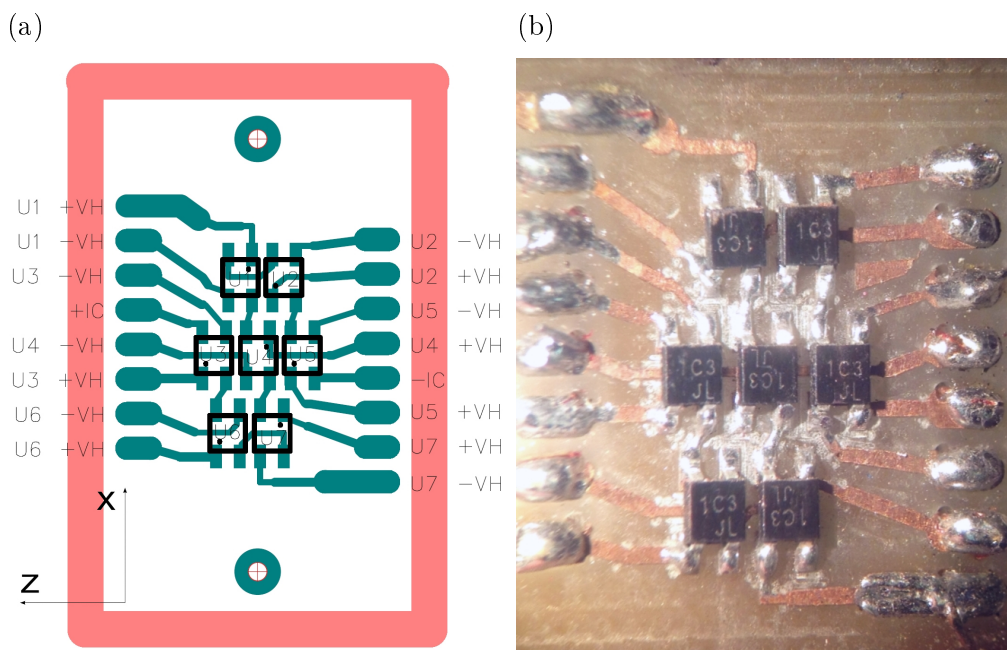measurements

(a)   (b)

Figure 2.4: (a) Draft and (b) picture of a sensor head with seven Hall probes; the first
line (1,2) is shifted by 1.6 mm and the third (6,7) by 0.8 mm from the left
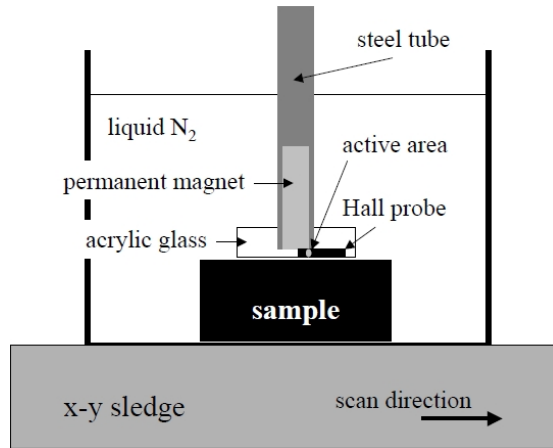side compared to the second line (3,4,5)

Figure 2.5: Schematic of magnetoscan setup [42]

of $10\,\mu m$ in the x and y-directions, usually $50\,\mu m$ above the surface. The Hall voltage is measured by a Keithley 2700 voltmeter. The measurement is controlled and recorded by a computer. By mapping the field, local variations of J_c can be investigated.

3 YatesStar

3.1 Setup and Operation

YatesStar (YS*) is an apparatus, developed by J. Yates Coulter [1–3] at the Superconductivity Technology Center (STC) at Los Alamos National Laboratory and further developed at the ASC/NHMFL [9, 44] to make transport critical current measurements of long tapes at 77 K. The tape incrementally unwinds from a feed reel and gets wound on the take-up reel, controlled by two SmartMotors from Moog Inc., Animatics. In between, two Ag-clad pulleys support the tape transport and serve as current leads for the transport current measurements. Furthermore, on the axis of these pulleys, external encoders connected with the motors record the tape position. YatesStar is shown in 3.1 (a) and a schematic diagram of its method of operation in 3.1 (b).

If the tape is moved forward, Motor 2 applies a constant torque and Motor 1 unwinds the tape. In backward direction it is vice versa. Through this process it is guaranteed that the tension of the tape is kept in between the two reels and the tape cannot fall off its holder. Due to the decreasing radius of the tape on the feed reel during the measurement the velocity of the tape decreases as well, since the velocity of the motor is constant. Without a regulation of the velocity of the tape, the resolution in length increases during the measurement and extends the measurement duration.

In between the current pulleys two permanent magnets on rotatable bearings, with a maximum field of ≈ 0.53 T and a DC electromagnet capable of 1 T are mounted. The field of the electromagnet can be adjusted with a current source and is usually set to the same field as the permanent magnets to produce the same conditions for the measurements. Its field is parallel to the c-axis of the superconducting tape. The permanent magnets can be rotated so that their field lies in the ab plane or is parallel to the c-axis of the conductor. The tape is moved through the center of the field of the magnets. The magnets are located between two voltage tabs, respectively. Usually the distance between the voltage tabs is important for measuring the I_c using the usual $1\,\mu V/cm^{-1}$ criterion. In this case the applied magnetic field locally reduces the I_c and the voltage drops outside the field maxima are negligible. The length of the field homogeneity is about 2 cm each and this dimension is used for the calculation of I_c. Three small pulleys ensure an electrical contact between the tape and the voltage tabs. These in-field measurements not only allow measurements with weaker transport currents but also prevent tape damage between the current leads and the outer voltage tabs, since the critical current density outside the field is higher. Damages reduce I_c, but only major defects lower the critical current as far as the field does.

The measurements are controlled via a Visual Basic program. It controls the tape movement, the ramp rate and the maximum amount of the applied transport current

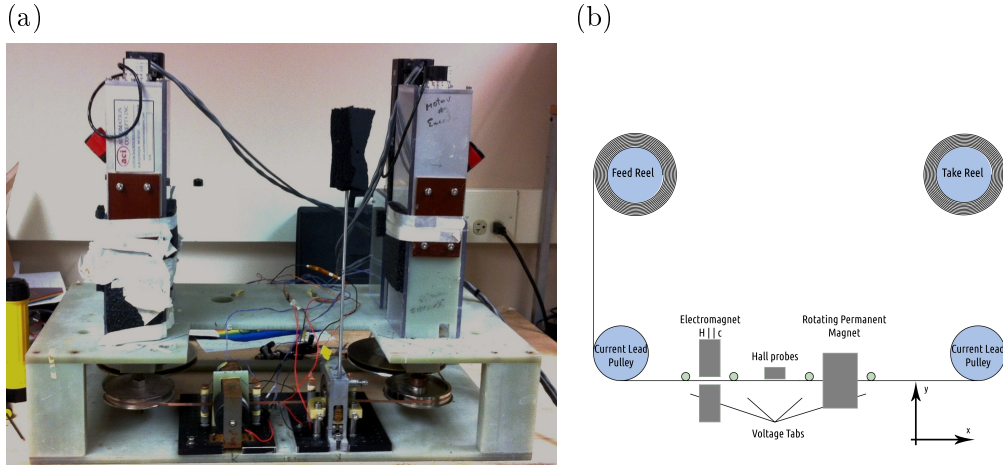(a)   (b)

Figure 3.1: (a) YatesStar and (b) schematic diagram of the apparatus

and measures the voltage drops versus position. Further it calculates automatically the I_c and n-values. A short break between a step of movement and the transport current measurement substantially reduces the noise.

During the measurement YatesStar is situated in a bath of liquid nitrogen, which is insulated with several layers of Styrofoam on the bottom and the edges. To reduce thermal losses the open cryostat can be covered with a sheet of perspex and another layer of Styrofoam, both trimmed to fit the motor and encoder/current pulley towers. Since measurements with a very high resolution up to 2 cm and a total tape length of more than 100 m could take from several hours up to two days, a good thermal insulation is needed. Improvements increased the time between nitrogen refills substantially to 6-8 hours.

3.1.1 Four-Point Method

If the resistance of electrodes is approximately of the same order of magnitude, or even larger then the signal itself, it is necessary to perform four-point measurements, a technique that uses separate pairs of current-carrying and voltage-sensing electrodes. This separation eliminates the impedance contribution of the wiring and contact resistances. The accuracy of the technique comes from the fact that almost no current flows in the sensing wires, so the voltage sensitivity in measuring E is high.

3.1.2 I_c and n-values

YatesStar automatically calculates two important parameters for the analysis of superconductors, $I_c(x)$ and the parameter $n(x)$ from a power law $V \propto I^n$ for a certain position x. $I_c(x)$ depends on the local critical current density $j_c(x)$ and the superconducting cross section $A(x)$. However, n only depends on J_c. Therefore it is possible to distinguish between local variations in the cross section or in J_c. If both parameters show the same local behavior the variation is caused by changes in J_c. On the other hand, if only the I_c value changes, it corresponds to a de- or increasing cross section [1]. The critical

23
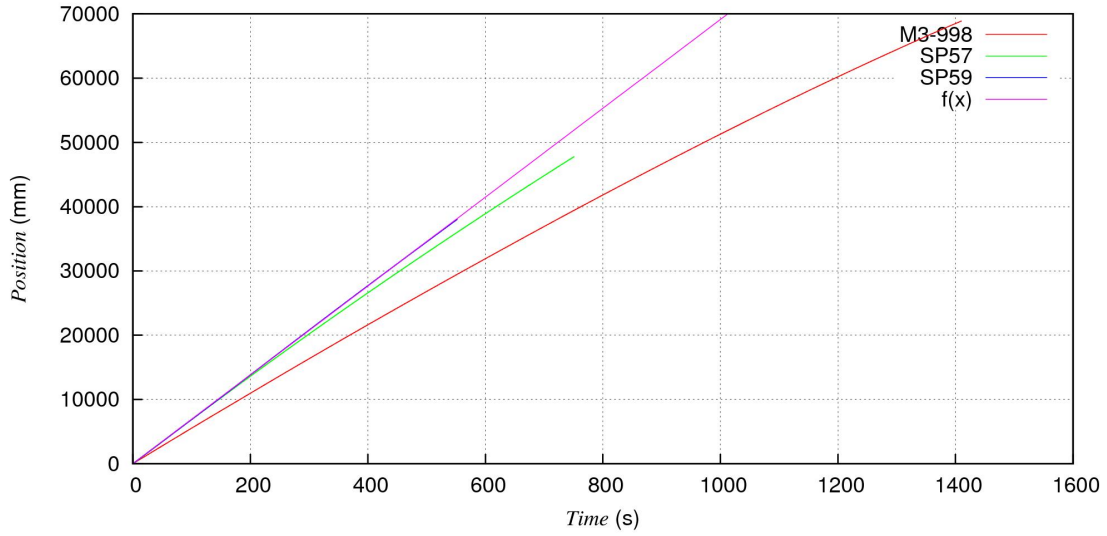
Figure 3.2: Position of the tape over time for three different measurements and a linear function $f(x)$; the velocity for the measurements of SP57 and SP59 was corrected continuously

current density depends on the microstructure of the CC. n is fitted to the I-V curve between $1\,\mu V$ and $50\,\mu V$. The voltage drop is caused by motion of flux vortices and the superconductor remains in the superconducting phase.

3.2 YatesStar 1.1

In the following subsections I will discuss new developments, both hardware and software, made in the last few months during this work.

3.2.1 Sensor Head Holder

A simple construction was built to mount the Hall probes at the base frame of YatesStar. The height of the Hall probes and the distance between the sensors and the tape surface are adjustable. Vertical up and down motion of the tape can modify the measured signal very strongly. A tape stabilizer is necessary to suppress those fluctuations in tape height (z direction) and was added subsequently. No less important is a constant distance d between the Hall probes and the tape, since the magnetic field decreases as $1/d$. However, a stabilization in y direction is more difficult due to variations in the tape thickness (coupling joints to copper leader). Increasing the tension can stabilize the tape but may cause also more friction on the fixed tape guides which can damage the tape.

3.2.2 Position Calculation and Velocity Correction

The velocity of the tape is defined by the velocity of the feed motor and the instantaneous radius of the tape on the spool. As the tape unspools, its decreasing radius leads to a decrease in the velocity of the tape. Since we are using two different systems to control the motors and measure the voltage of the Hall probes over time, we have to recalculate the time-dependent position. We are starting with the velocity v_0

$$v_0 = \frac{2\pi r}{t}, \tag{3.1}$$

with an outer radius r of the spool/tape at time t. Simplified the outer radius decreases after one revolution by the thickness of the tape dr leading to a velocity v_1

$$v_1 = \frac{2\pi(r - dr)}{t}. \tag{3.2}$$

After i revolutions the tape velocity is

$$v_i = \frac{2\pi(r - idr)}{t} = v_0 - \frac{2\pi idr}{t}. \tag{3.3}$$

If t is the time of one revolution of the motor, the position of the tape after i revolutions is

$$P_i = P_0 + \frac{1}{2}\sum_{j=0}^{i-1}(v_j + v_{j+1})t = P_0 + 2\pi ir - i^2\pi dr. \tag{3.4}$$

i results from the total duration of the measurement and the constant turning velocity of the motors, or if known, from the difference between the final and initial value of the internal encoder divided by counts per revolution (=2000 in our SmartMotors). r and dr can be measured by ruler or can be fitted to position data from the system which controls the motors. The thickness of the tapes is in the order of 0.1 mm - 0.18 mm. This allows us to use the simplified model with a very small error. A geometrical approach validates our assumptions. A tape is wound on a spool. The covered area within an inner radius r_i ($r_i \neq r_i$) and an outer radius r_o is

$$A = (r_o^2 - r_i^2)\pi = l \cdot dr. \tag{3.5}$$

With $r_o = r_i + i \cdot dr$ and $r = r_o$ follows

$$l = P_i - P_0. \tag{3.6}$$

A constant velocity of the tape could be reached 1.) if the velocity of the motor is adjusted by time considering the decrease of the radius, or 2.) the motor speed is controlled by the external encoder. The second has been tried first, but the internal control and feedback functions were insufficient and a safe measurement was not ensured. Therefore, we added a velocity correction to the motor control software, such that the tape velocity v then

stays constant, by increasing the motor velocity s. The time t per revolution is then no longer constant. Simplifications like the above lead to

$$s_i = s_0 \frac{1}{1 - i\frac{dr}{r}}, \tag{3.7}$$

with s_i as the velocity of the feed motor after i revolutions. In figure 3.2 the position over time is shown for three different measurements. In case of the longest tape M3-998 we did not use any velocity correction. Therefore the velocity of the tape is decreasing as the measurement proceeds. For SP57 we already used the correction explained above, but the fit parameters r and dr were badly estimated. For the shorter tape SP59 with a length of about 38 m the parameters were measured more precisely and the correction leads to an almost constant tape velocity, as the comparison with the linear function $f(x)$ shows. The slope of $f(x)$ is the initial velocity of the tape.

3.2.3 Extension to Helium Measurements

Helium is rare on earth and the price for liquid helium is much higher than for liquid nitrogen. Filling the cryostat of YatesStar with liquid helium instead of liquid nitrogen is not feasible. Hence, for continuous tape measurements at 4.2 K we had to fit our measuring equipment into a 52 mm wide magnet bore and build an extension to ferry the tape into the center of a solenoid magnet inside the cryostat. Transport current measurements are not compatible with such conditions, because the critical currents at low temperatures are far beyond 1 kA and for such currents the necessary thickness of the current leads exceeds the given space. On the other hand, magnetization measurements are promising. We developed an extension for reel-to-reel magnetization measurements inside a magnet bore. A schematic of the setup is shown in figure 3.3. YatesStar is mounted on the top of the cryostat and the tape is transported into the bore, guided by several small pulleys. A magnet produces a vertical field of up to ∼15 T inside the bore. In the center of the magnet, where the field has its maximum, the tape gets magnetized. Above the magnet but still in the cryostat, the remanent field of the tape is measured with Hall probes. The height of

Figure 3.3: Schematic of the setup for measurements in liquid helium

the Hall sensors above the solenoid is determined by two contrary requirements: a sufficient distance to the magnet is necessary to avoid significant stray fields and on the other hand the height defines the minimum helium fill level of the cryostat. Additional to the

internal helium level indicator of the cryostat a thermometer monitors the temperature 5 mm above the Hall probes. Precooling the tape with liquid nitrogen is not necessary, nor is heating the tape when it gets back out of the dewar due to the temperature gradient inside the cryostat. This setup enables continuous reel-to-reel measurements with low helium consumption (without any field, the sealed cryostat consumes ∼2 % per hour compared to ∼3 % per hour during our measurements). Tapes can be changed quickly, as long as a copper leader is left through the magnet. The most critical issue of the construction is the essential leader. Due to the bending in the center of the magnet weak coupling joints between leader and tape are susceptible to breakage. Additional Hall probes at the turning point can measure the in-field behavior of the superconductor. The bending diameter (42 mm) in this apparatus is larger than the critical bending diameter (11 mm) of the tape according to SuperPower by a factor of 4.

3.3 Data Evaluation

The Hall probes measure the magnetic field at a finite distance from the surface of the superconductor. Obvious defects can be seen at a two dimensional field map. There are several methods to calculate the critical parameters of the tape, described below. The field in the center of the tape is symmetrically influenced by all currents flowing across the tape width. Any inhomogeneities in the critical current density J_c in z direction affect the measured field in the center [45]. Therefore the field distribution along the tape length in the center of the sample is proportional to the critical current I_c, as shown later.

3.3.1 Position Determination

In the early measurements we were not able to record the tape position during the Hall scans. To compare the data of the transport current ($I_c(x)$) and the magnetization ($U_H(t)$) measurement we first have to determine $x(t)$ with equation 3.4 to get $U_H(x(t))$. The number of revolutions i can be subsequently calculated by division of the total measuring time T (time of tape movement) by the time per revolution t. Since the total length of the superconductor is known, the parameters r and dr can be fitted to match the beginning and end points.

A temporary solution provides two separate measurements of the position and the Hall voltage with different measuring rates, but the same duration. The total number of measured position points is p, the number of voltage points is q. Since the ratio $p/q \approx 1$, a linear interpolation gives a sufficiently good result for providing q position points.

A software solution based on LabVIEW which controls the motors and reads the voltmeter is still under development.

3.3.2 Assessment of I_c

A widely used method to assess the critical current is to calibrate the Hall probe system. After measuring the whole tape with Hall probes a short sample at one end of the tape is

cut and its critical current measured. A calibration factor c' (AV^{-1}) is determined, which links the Hall voltage signal to the critical current by the linear relation $I_c = c' \cdot U_H$. With equation 2.3 we can write $I_c = c \cdot B$ with a factor c (A/mT). Since we are measuring the local $I_c(x)$ over the full length of the tape, we are able to calibrate the Hall measurement in a non-destructive manner. The evolution of the local calibration factor $c(x)$ gives information about variations of the ratio of the in-field and self field I_x.

3.3.3 Evaluation of J_c

The measurement with several Hall probes across the width of the superconducting tape allows us to analyze the field profile of the tape. According to Bean's critical state model (section 1.4) J_c corresponds to the slope of the magnetization in z direction. Although Brandt and Indenbom [46] showed that this assumption is not valid for flat superconductors in a perpendicular field due to demagnetization effects, the application of this model should provide the order of magnitude. The slope m can be calculated by a linear regression of the field profile

$$m = \frac{n \sum\limits_{i=1}^{n} (z_i \cdot B(x, y, z_i)) - \sum\limits_{i=1}^{n} z_i \sum\limits_{i=1}^{n} B(x, y, z_i)}{n \sum\limits_{i=1}^{n} (z_i^2) - (\sum\limits_{i=1}^{n} z_i)^2}, \tag{3.8}$$

where z_i is the vertical position of the Hall probe i (tape ab-plane is in the x, z-plane), y the distance between the Hall probes and tape surface, $B(x, y, z_i)$ the field at the position (x, y, z_i) and n is the number of Hall probes, which are used for the regression. The orientation is consistent with the coordinate system introduced in figure 3.1 (b) and figure 2.4 (a). Obviously, the regression is made only over one half of the tape (HP a - d & HP d - g).

3.3.4 Evaluation of I_c

Based on Ampère's circuital law, we can find the Biot-Savart law for one dimensional (in x direction), thin strand current distributions

$$\vec{B}(\vec{r}) = \frac{\mu_0}{4\pi} I \int \frac{\mathrm{d}\vec{s} \times \hat{r}}{|\vec{r} - \vec{r}'|^2}, \tag{3.9}$$

with $\hat{r} = \frac{\vec{r} - \vec{r}'}{|\vec{r} - \vec{r}'|}$. The Hall probes measure only the field in y direction. Therefore we carry out the cross product and calculate only B_y. With $\mathrm{d}\vec{s} = \mathrm{d}x' \cdot \hat{e}_x$ we can write

$$B_y = \frac{\mu_0 I}{4\pi} \int\limits_{-\infty}^{\infty} \frac{z - z'}{\sqrt{(x'^2 + (y - y')^2 + (z - z')^2)^3}} \cdot \mathrm{d}x'. \tag{3.10}$$

28

The calculation of the integral delivers an expression for the magnetic field of an infinitely long, straight wire in the x direction

$$B_y = \frac{\mu_0 I}{2\pi} \frac{z - z'}{(y - y')^2 + (z - z')^2}.$$ (3.11)

From now on we only consider the field in y direction and write B without an index for the direction. Further, we assume that only N discrete currents flow inside the sample. At position $r_i(x)$, the magnetic field $B_i(x)$, measured with the Hall probe i, is the superposition of all magnetic fields $B_{ij}(x)$, caused by the currents $I_j(x)$ flowing at $r'_j(x)$:

$$B_i(x) = \frac{\mu_0}{2\pi} \cdot \sum_{j=0}^{N} \frac{(z_i - z'_j) \cdot I_j(x)}{(y_i - y'_j)^2 + (z_i - z'_j)^2}$$ (3.12)

The origin is chosen to be at the position of one of the edge Hall probes. Thus the coordinates for the other Hall probe positions and the suggested discrete current distribution are given by $\vec{r}_i = i \cdot \Delta z \cdot \hat{e}_z$ and $\vec{r}_j{}' = \Delta y \cdot \hat{e}_y + (j - \frac{1}{2}) \cdot \Delta z \cdot \hat{e}_z$, with Δy as distance between the sample surface and the Hall probes and Δz as distance between the active area of two Hall probes.

For m measuring points $i \in [1, m]$ and n currents $j \in [1, n]$ one can write

$$\vec{B} = \underline{A}\vec{I},$$ (3.13)

with the matrix $\underline{A} \in R^{m \times n}$. This system of linear equations can easily be solved with several algorithms, if $n = m$. It is important to note that $\vec{B}$ is an m-dimensional vector with values B_i at different positions i. It does not match the three dimensional magnetic field vector. The solution of equation 3.13 is the required current distribution.

4 Samples

All tested samples were produced by Superpower Inc. for use in various magnet projects at the NHMFL. A typical conductor architecture of a REBCO 2G (2nd generation) HTS coated conductor is shown in figure 4.1. The superconductor consists of (RE)BCO. On a Hastelloy (nickel-molybdenum-chromium alloy) substrate with a thickness of $50\,\mu$m, a multi-oxide buffer stack is deposited. The first buffer stack, consisting of alumina, serves as diffusion barrier against Ni poisoning of the REBCO by the substrate. The grains of the substrate are all differently oriented. To reach oriented growth, a MgO buffer stack with oriented grains in z-direction (c-axis) is grown by ion beam assisted deposition (IBAD) on a Y_2O_3 seed. A homo-epitaxial MgO layer improves the texture and the fifth layer is the $LaMnO_3$ cap layer [39], which matches the lattice parameters of the HTS layer. The REBCO layer grows epitaxially by metal organic chemical vapor deposition (MOCVD). These complex processes aim at minimizing the angles between the grain boundaries to increase the critical current density. The thickness of the YBCO layer is limited by the finite epitaxial growth, leading to a loss of the crystallographic orientation at large thickness ($\gg 1\,\mu$m). A thin cover layer of silver is sputtered on the YBCO layer to provide good electrical contact. A copper surrounding of $20\,\mu$m thickness serves as stabilizer of the conductor. In all tapes $BaZrO_3$ nano particles are added to improve the vortex pinning behavior.

SuperPower Inc. uses several machines for manufacturing coated conductors. The first two characters in the SuperPower label of a tape refer to the respective machine (e.g. M3 to machine 3). The tape is produced on a $12\,$mm wide substrate and the finished conductor is slit in three parts. The labels FS, MS and BS refer to front slit, middle slit and back slit, respectively. A schematic is shown in figure 4.2. This graphic anticipates the width variations we found in the samples and links it to the slitting process. An overview and summary of the measured tapes is given in table 6.1 on page 56. The table lists the SuperPower Inc. and NHMFL in-house "SP" labels, the conductor lengths and the numerical results of the characterization of the tapes.
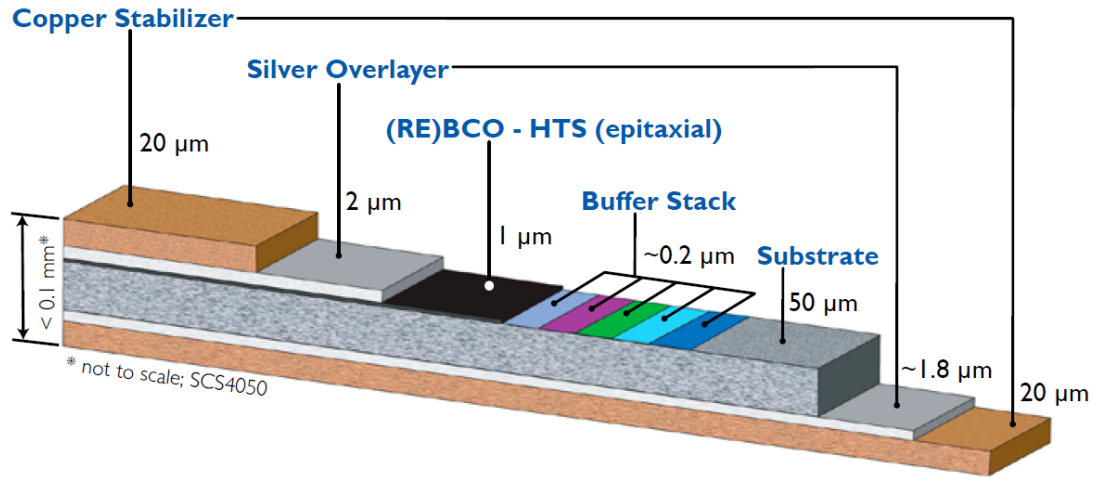
Figure 4.1: Typical sample architecture of a 2G HTS MOCVD/IBAD coated conductor from SuperPower Inc. [47]
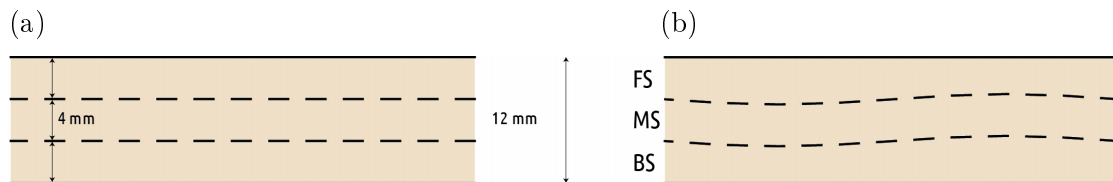
Figure 4.2: Slitting process of a 12 mm wide tape: (a) ideal: three equidistant parts, (b) real: the slitting process causes variations in width (disproportionately pictured) with a period of about 28 cm

5 Results

We continuously adapted and improved our measurement system, which increased the quality and reliability of our measurements. I will present in this chapter the results mostly in chronological order with explanations of the development process. Especially in the beginning, we experienced several problems with YatesStar itself, which, I would like to emphasize, is still in the status of a prototype, but also with our new development of the Hall probe measuring system. Due to a tight time schedule in the groups which provided the samples, we only had a limited time period to test the tapes and multiple test runs were not always possible. The measurement itself takes up to three days for samples above 100 m. Further the construction of YS* requires the whole apparatus to be cooled. Therefore the whole apparatus has to be warmed up as well, when the tape is changed. The present mounting configuration of the two pulleys makes them vulnerable to freezing. According to our experience, a pause of at least two days between warming up and cooling ensures that all the water, which was absorbed in YS, is released again and prevents freezing of the pulleys. Reversing the direction of the movement was not always possible, because the tape easily looses its tension and could fall off of its spool.

5.1 Tape M3-747

On this first tape we measured the critical current I_c via transport current measurements and the remanent field with Hall probes simultaneously. As described in chapter 3 the cycle of local $I_c(x)$ measurement takes approximately 30-35 s. This is clearly observed with the Hall probes. Figure 5.1 shows one of those cycles. The first vertical bar at 3.5 s indicates the point when the tape starts to move and the second when it stops. During a pause of ≈ 17 s relaxation can be observed. At the third bar the current ramp starts. To speed up the measurement, there is a jump in the transport current from 0 to 20 A. Then the current is increased at a constant rate. This transport current flowing in x direction produces a magnetic field (Ampère's circuital law):

$$\vec{\nabla} \times \vec{B} = \mu_0 \vec{j}. \tag{5.1}$$

The Hall probe array is mounted in the positive y direction (the tape is mounted with vertical ab-plane). Therefore the superposition of the remanent field and the field caused by the transport current reduces the local field at the position of the top Hall probe (in z direction) and increases the field at the Hall probe at the bottom. The Hall probe measures the field perpendicular to the ab-plane of the superconductor and the transport current produces an azimuthal field. If the central HP is mounted exactly above the center of the tape, the current ramp could not be observed. As seen in figure 5.1

(a)

(b)
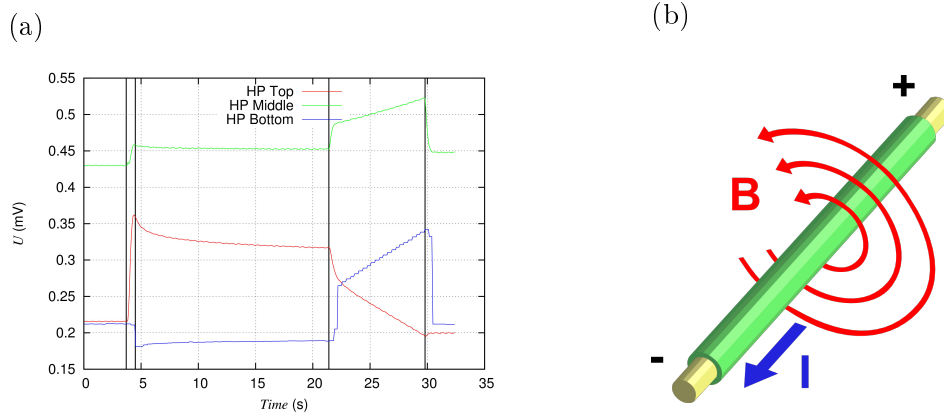
Figure 5.1: (a) One cycle of a local $I_c(x)$ measurement; (b) visualization of Ampère's law for a straight current carrying wire[1]
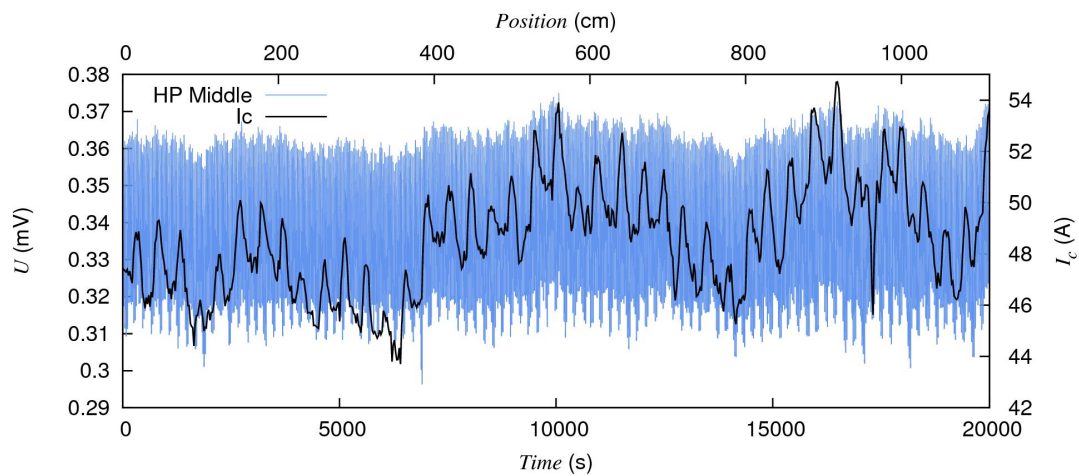
Figure 5.2: M3-747: The I_c curve from transport current measurements compared to the central Hall probe signal; long fluctuations correlate obviously

(a), the central HP (HP Middle) observes the transport current. Therefore its position is slightly shifted compared to the center of the tape in the direction to the Hall probe at the bottom.

In figure 5.2 several hundred cycles are shown and compared to the I_c data. The origin in time and position is arbitrary. A correlation of long fluctuations is obvious. To extract more information out of thousands of data points, an algorithm would be needed to separate the different parts of those cycles. The variations in the duration of the cycles lead to a difficult evaluation. An automatic separation by looking for local maxima did not achieve good results. Two independent measurements of the I_c and the remanent field greatly facilitates the evaluation.

Figure 5.3 shows the I_c over the full length of the conductor. Due to a failure of

---

[1]Published under terms of GNU Free Documentation License by its author User:Stannered, wikipedia.org
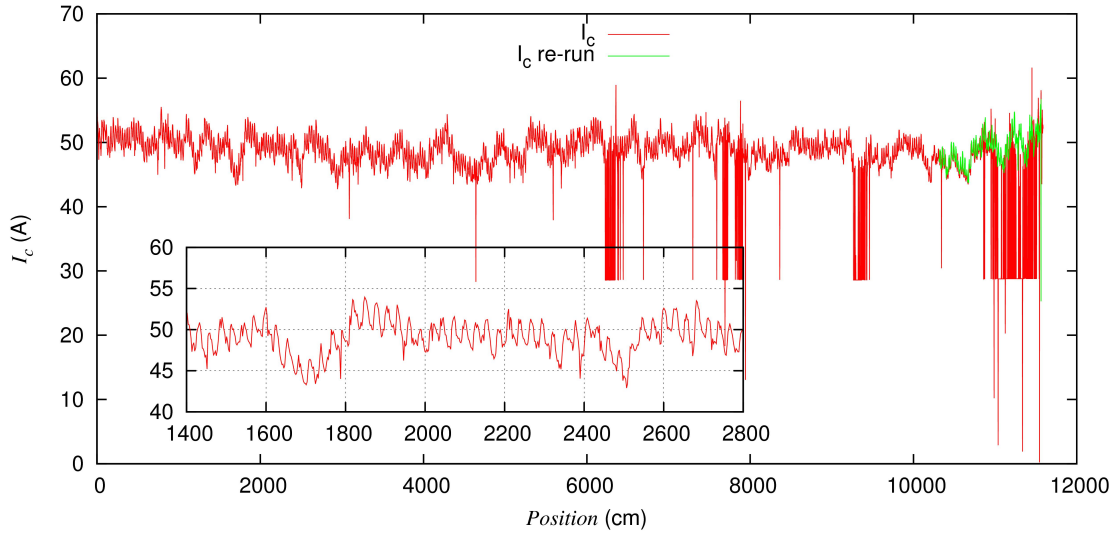
Figure 5.3: M3-747: I_c measured over the full length of tape, several errors occurred after 60 m (large dropouts), a re-measurement (green) of the last 12 m confirms that dropouts are due to a dysfunction in the measurement and damaged areas in the tape; inset shows short fluctuations over 14 m

the electromagnet, only one channel was measured. After 62 m several errors occurred. A re-run of the last 12.5 m proves, that the dropouts are not real. The tape was not destroyed in these areas. However, errors also occurred in the end of the second run. The reason for those errors was not discovered, but might be due to one or two bad contacts between the voltage taps and the tape. The drops are going down to $\approx 28\,\mathrm{A}$, but this value is slightly increasing over the length of the measurement, which is not understood. The drop to a nearly constant value is caused by the speed up function, which shortens the measurement time by starting the current ramp not from 0 A, but from a set value $I_{\mathrm{speed\ up}} > 0\,\mathrm{A}$. Bad spots with an I_c below the speed up current can not be resolved and the $I_c(x)$ will be defined as $I_{\mathrm{speed\ up}}$. $I_{\mathrm{speed\ up}}$ was set to 20 A for this measurement.

The $I_c(x)$ consists of a superposition of long and short fluctuations. The inset of figure 5.3 shows the short fluctuations with a length of $\approx 27.5\,\mathrm{cm}$. These fluctuations were already observed in previous measurements and are found to correlate to width variations of the tape, which are very likely caused by the slitting process. The circumference of the disk knife, used to slit the tape, is about 28 cm. As mentioned above, simultaneous measurements of I_c and the magnetization makes the evaluation complicated. The continuous Hall measurements are much faster, so we were able to measure the tape again. In figure 5.4 the result of the magnetization measurement (right scale) is shown and compared to the I_c data (left scale). There are position uncertainties of about $\pm$ 10 cm, but a very good correlation is observed. The Hall signal comes from the central Hall probe, which was approximately above the center of the tape. The value of the Hall probes

34

above the copper leader was assumed to be the offset and is taken into account by the evaluation. The voltage signal is further divided by the Hall coefficient and the driving current. The green and the magenta lines indicate linear fits to the two measurements. To do so, the drops to 28 A are removed in the plotted I_c data and used to calculate the linear fit of I_c. The mean I_c of this tape is 48.80 A at 0.53 T with a standard deviation of 2.36 A. The local I_c average is slightly decreasing over the length at a rate of 9.21 mA/m. The Hall signal decreases too, but faster with 14.29 µT/m. Therefore it is not possible to calibrate the Hall measurement only at the beginning of the tape. The local calibration factor is $c(x) = 4.01 + \frac{4x}{1000}$ A/mT, where x(m) is the actual position. Short samples cut from the beginning and the end of the tape were measured by Dr. Dmytro Abraimov in self field: $I_{c,sf}(x = 0\,\text{m}) = 143$ A and $I_{c,sf}(x = 116\,\text{m}) = 136$ A, respectively. The rates of decrease in permill per meter for the self field, the reel-to-reel in-field and magnetization measurements are 0.4 ‰/m, 0.2 ‰/m and 0.7 ‰/m. We would expect similar rates for the magnetization and self field methods. The difference might be explained by the fact, that the linearization of the self field I_c was calculated only from the results of the measurements on two short samples with a length of ≈ 12 cm each. The fluctuations of $I_c(x)$, observed in the in-field measurements, are already in the range of a few amperes. Those long fluctuations cannot be seen in the short sample characterization. Therefore, with an uncertainty of 2 A the rate of decrease would increase to 0.6 ‰/m. Assuming that the magnetization method corresponds to the self field I_c, we find that fluctuations and defects occur under both circumstances (in-field and self field), but some processes during manufacturing or other unknown effects cause different rates of decrease.

The inset shows a length of 14 m in detail. Two small dropouts at 5600 cm and 5700 cm are observed in the I_c measurements as well as with the Hall probes, but are shifted in position by 22.9 cm. The large dropouts at ≈ 77 m, 93 m, 103 m, 111 m and 113 m are not observed with the Hall probes and might not be real. On the other hand, the drops to 38.1 A at 30.9 m and to 37.8 A at 55.9 m are seen in both measurements independently and we conclude that these bad spots are real. These dropouts show the importance of the double measurement for the reliability of the results. The average of the measured field is 11.41 mT with a standard deviation of 0.73 mT. We can further compare the ratio of the standard deviation and the average of the magnetization and the critical current measurement, which is 0.064 and 0.046, respectively. In figure 5.5 the current distribution of this tape is shown. The currents are normally distributed (Gaussian distribution), but the quench behavior is mainly determined by the minimum I_c. The width of each box is 0.4 A.

It has to be mentioned that both of the pulleys froze during the I_c measurement, forcing the position to be recalculated. The measured position and the calculated position are shown in fig. 5.6. To determine the real position, the measured position from 0 to 64 m was fitted to equation 3.4. The measured position stuck after 64 m because the pulley froze. It was deiced a few hours later. The fit parameters were than used to calculate the red line. This position data was used in the results presented above.
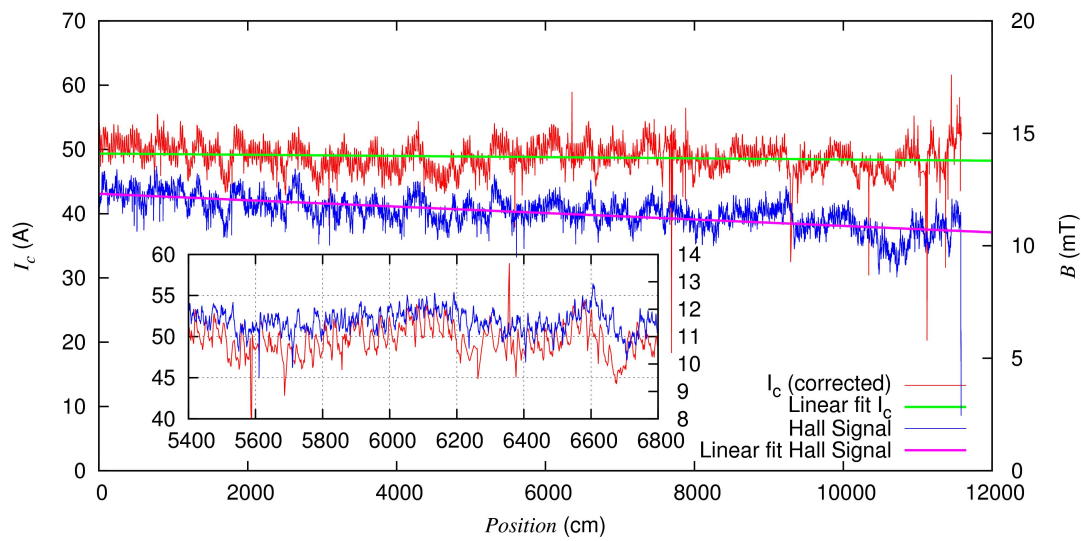
Figure 5.4: M3-747: Comparison of two measurement methods over nearly 120 m; the I_c and magnetization data correlate very well
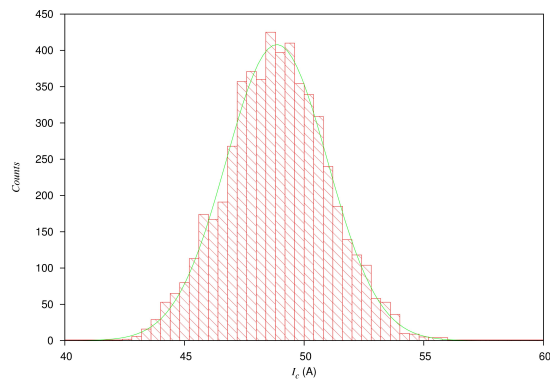
Figure 5.5: M3-747: Critical current distribution of the tape, a Gaussian function describes it very well
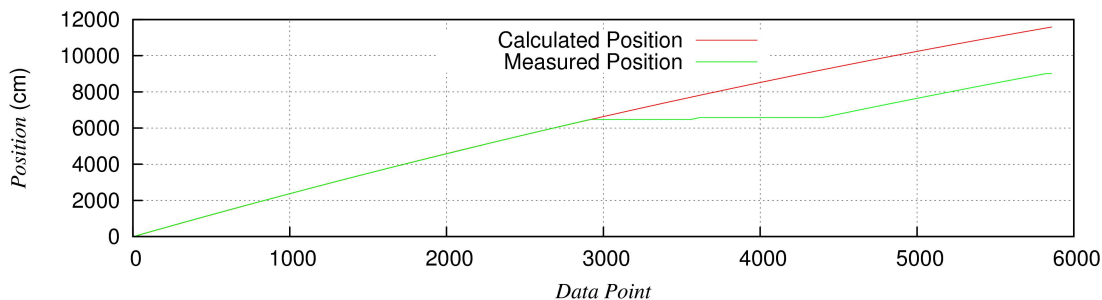
Figure 5.6: Measured and corrected position of M3-747 I_c during the transport measurement

5.2 Tape M4-52

The next tape measured in full length was M4-52 from Superpower. This tape is also used for a superconducting magnet project at the National High Magnetic Field Laboratories. The knowledge of the I_c profile of the tape is crucial to improve the analysis of the quench behavior of the magnet. Several pairs of voltage tabs were fixed to the tape during the magnet winding process. With the provided data, shown in figure 5.7, magnet engineers were able to monitor special regions by measuring the voltage drop, where a quench is more probable during a test.

The behavior of the $I_c(x)$ over the length is not as clear as in tape M3-747. The linear fits of the data are split in two parts ($<$ and $> 65\,\mathrm{m}$). Below $65\,\mathrm{m}$ the critical current is slightly increasing. The same behavior was measured with the Hall probes. The signal is increasing with a similar slope. In the second length the mean I_c is strongly decreasing with increasing deviations. The Hall signal decreases as well, but much slower. The in-field I_c at the end is about $5\,\mathrm{A}$ lower than at the beginning. However, the magnetization decreases to the initial value. For a more detailed characterization of this tape, short samples were cut at the beginning and the end and their self field I_c at $77\,\mathrm{K}$ was measured by Dr. Dmytro Abraimov, yielding results of $112\,\mathrm{A}$ and $111\,\mathrm{A}$. The self field I_c decreases by less than $1\,\%$ and corresponds to the decrease of the magnetization. The in-field I_c decreases by $\approx 11\,\%$. We already found different rates of decrease of $I_c(x)$ in M3-747, but in this tape the in-field I_c decreases much faster.

The inset of fig. 5.7 shows the development of the standard deviation of the transport current measurement. The error bar in x direction indicates the region over which it was determined. In the Hall measurement one bad spot occurs at $57.5\,\mathrm{m}$ as measured by two different Hall sensors. It drops to $70\,\%$ of the average of its closest neighbors. If this drop is real, the tape could have been damaged, while the tape was spooled back to the beginning for the start of the magnetization measurement. Since it was not observed in the I_c measurement it could be an artifact on the surface of the tape as well. For safety reason a voltage tab was recommended in this section of the tape during magnet tests.

To compare the quality of this tape with the M3-747, we can look at the ratio of the standard deviation and the mean value. A small number is desirable, which implies a
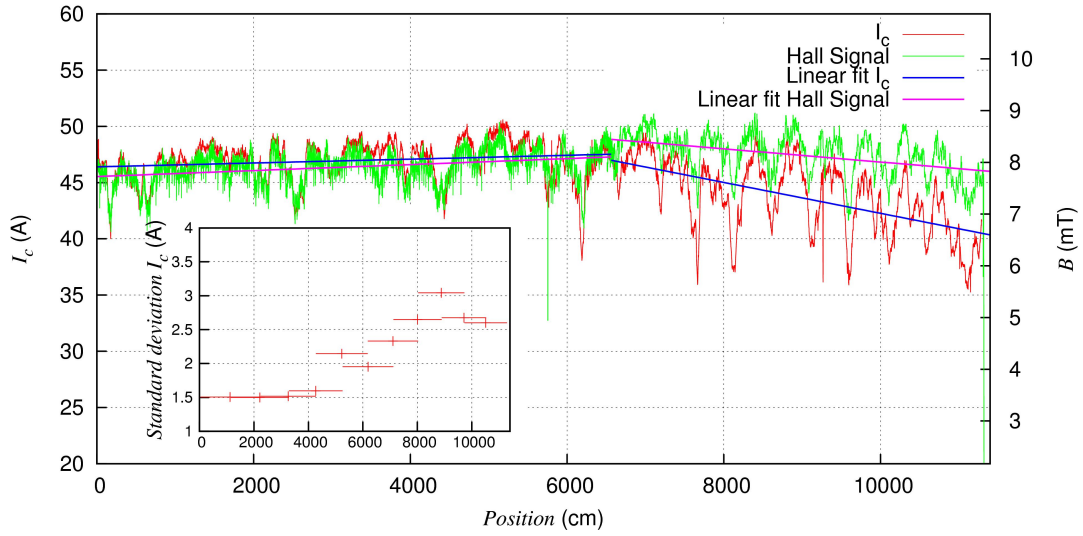
Figure 5.7: Results of I_c and Hall probe measurement of tape M4-52, with linear fits for two sections each ($<$ and $> 65\,\mathrm{m}$); the inset shows the standard deviation of the I_c measurement for several regions

high mean I_c with small variations. Over the full tape the ratio is 0.067, compared to the M3-747 tape with 0.046, which is almost 50\,% higher. However, the ratio for the first half is only 0.036 (see table 5.1). This shows that further improvements in the production process are necessary to ensure better quality of the superconducting layer over the full length.

	Mean I_c (A)	Standard deviation (A)	Standard deviation/Mean
Full length (113 m)	45.4	3.046	0.067
1st half (56.5 m)	47.1	1.686	0.036
2nd half (56.5 m)	44.0	3.178	0.072

Table 5.1: Results of the I_c measurement on tape M4-52, where the tape quality decreases with length

5.3 Tape SP41

The 26 m long SP41 served as testing tape for the new measurement methods, both at 77\,K and 4.2\,K. Since this tape could not be used in any magnet project due to its short length and low I_c, we were allowed to destroy this tape in parts to see the accuracy of the measurements. Small defects like scratches only on the copper surrounding did not affect I_c nor the remanent magnetization as expected.
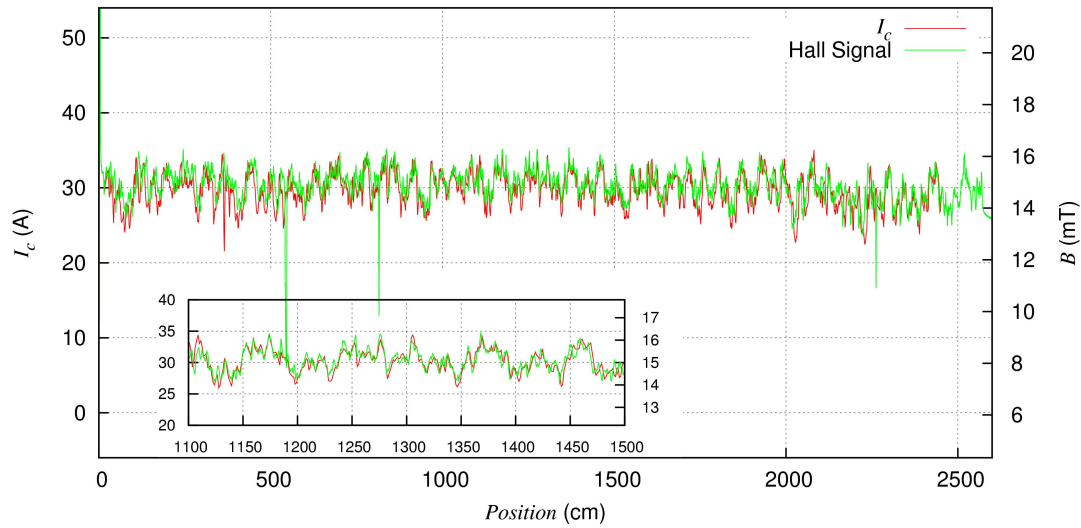
Figure 5.8: The I_c and magnetization profile of tape SP41 in the first series of measurements

SP41 was first analyzed by transport current I_c measurements and in a second run with the Hall probe measurement setup at 77 K. The results are shown in figure 5.8. In between those two measurements defects were added at 5.5 m, 8.1 m and 22.6 m by bending the tape. The defects are clearly observed in the magnetization profile in fig. 5.8. The Hall scan was performed over the full length of the tape, whereas in the transport I_c the last meters are missing. The mean I_c of the full tape is 29.6 A, and again the mean value of the I_c of the first half of the tape is higher than of the second. The average decrease is 45.2 mA/m, a gradient worse by a factor of five compared to M3-747, but it is not as obvious due to its short length. The calibration factor for this scan is c=3.6 A/mT and the self field I_c of the SP41 is 67 A.

5.4 Tape M3-998 (insulated tape)

The tape M3-998, with its 68 m length, was entirely insulated with polyester shrink tubes for its use in superconducting coils. The magnetization measurements are contactless and therefore allow us to analyze insulated tapes too. This feature is very interesting for the further development of insulation methods: by measuring the tape twice, before and after insulation, problems of the process can be determined and risks of damaging the tape can be avoided. In contrast, transport current measurements are not possible on insulated tapes.

For the first time we used the sensor head with seven Hall probes during this measurement. A much higher resolution across the tape width was achieved. Due to the higher resolution we found that the original tape stabilization was not sufficient. If the tape is not wound completely straight on the spool and the tape is not stabilized in vertical

(a) (b)
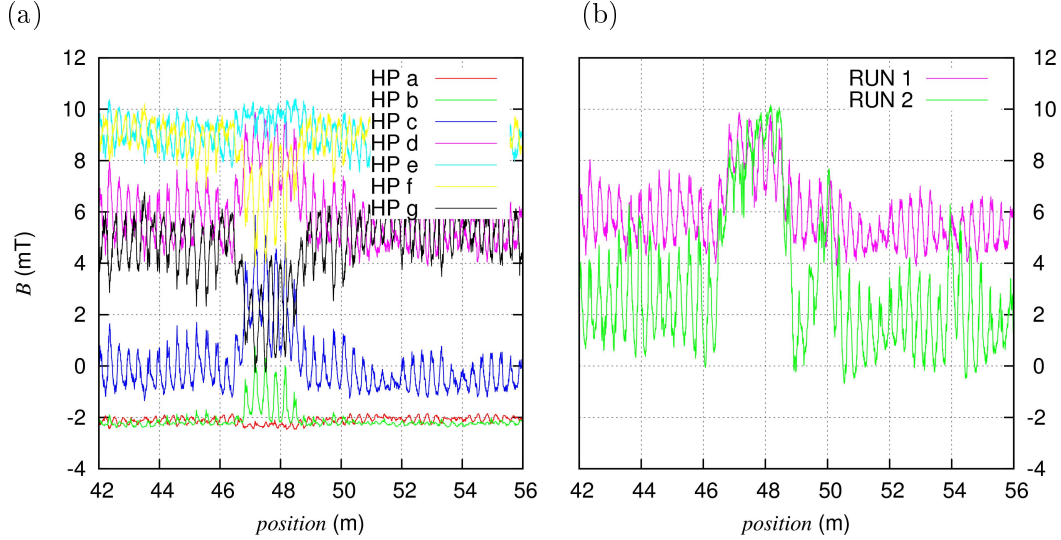
Figure 5.9: M3-998: Fluctuations in panel (a) are caused by the tape moving up and down (in the vertical direction) and not by mechanical or chemical destructions; (b) shows the reproducibility of those variations, which could lead to misinterpretations

direction it can move up and down slightly. This shift can lead to misinterpretations of the results, as shown in figure 5.9. Figure 5.9 (a) shows the signal of all seven Hall probes. The Hall probes are in vertical order from top (HP a) to bottom (HP g). The central Hall probe (HP d) was not fixed correctly above the center of the tape. The center of the tape, where the magnetization has its maximum, is rather between HP e and HP f. At meter 46 the tape moves a little bit towards the top. Big shifts in the signal strength are observed, which are only caused by a movement of several tenths of a millimeter. The Hall probes b, c, d and e register a higher field because they are getting closer to the field maximum, while the signal of the Hall probes on the lower edge decreases. Hall probe a, which is located on the upper edge of the array, was not above the tape and was barely influenced by the shifts. A repetition of this measurement leads to a similar result, shown in figure 5.9 (b). This reproducible shift aids and abets misinterpretations. A newly designed tape stabilizer improved the measurement setup.

The measurement was repeated and is compared to the first measurement in figure 5.10. The big drops between 40 m and 42 m and 65 m and 66 m vanish, as does the decay between 46 m and 51 m which is discussed above. A linear fit of the new result leads to a slope of 2.08 mT/m. The magnetization is slightly increasing. It has to be mentioned that the tape orientation might not be the original one and the same which is used for all the other tapes: beginning of the tape (at 0 m) is equal to the side where the production starts. The mean field is 8.18 mT with a very good ratio of standard deviation to mean value of 0.033. Since we changed the Hall probe array, the stabilizer and therefore the distance between Hall probe and tape surface, old calibration factors will not be helpful.
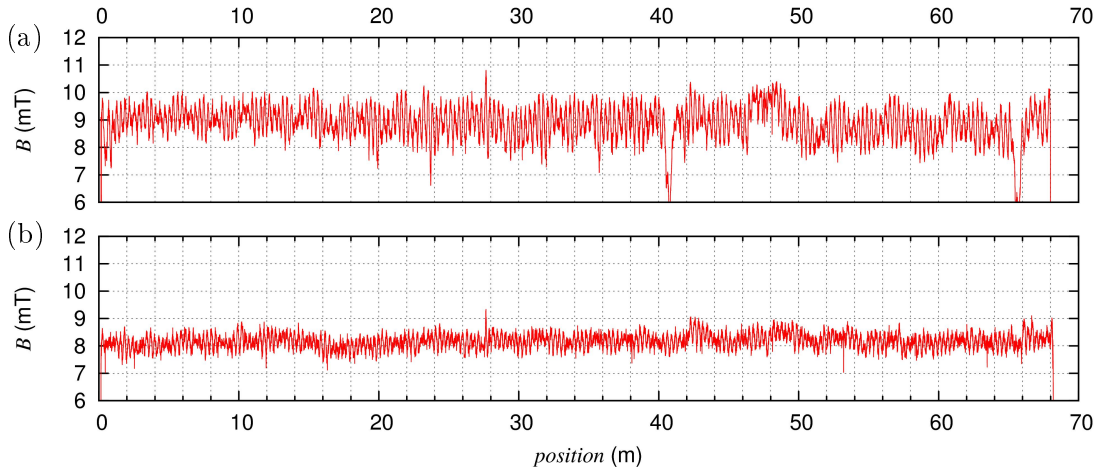
Figure 5.10: Direct comparison of two measurements on the insulated tape M3-998: (a) without a stabilizer in z-direction and fluctuations caused by variations of the tape height; and the repeated measurement (b) with a newly developed stabilizer; the weaker signal is probably caused by a larger distance between the tape surface and the Hall probe; (a) and (b) are showing the central line of the scan

The tape itself could not be measured absolutely by transport measurements due to its insulation. For this reason we soldered a collection of different short samples with different I_c values which are not insulated to the beginning of the tape M3-998. By measuring both the I_c of those short tapes and the magnetization profile, the Hall probe scan can be calibrated in situ. With this method the mean in-field I_c of this tape results in 56 A, corresponding to a calibration factor of 6.86 A/mT, which is almost twice the calibration factor for SP41. This is probably caused by a larger distance between the surfaces.

In this tape strong and fast fluctuations occur with a length of 28 cm, which again corresponds to fluctuations in tape width induced by the knife used in the cutting process. A 2D map of the remanent field profile is shown in figure 5.11. The central Hall probe (HP d) was not situated above the exact center of the tape, but close to it (several tenths of a millimeter). A more accurate manual positioning was not possible. Figure 5.12 shows five meters in detail. Variations in width are observed. This tape is a middle slit (MS), therefore both sides are cut and not straight. Actually it should reduce fluctuations, since the distance between the two disk knifes is maintained constant, but the center of the knifes is not kept straight over the center of the tape. This movement cause the 28 cm fluctuations in the I_c and magnetization curves. With seven Hall probes across the width of the tape, a field gradient can be calculated. Using equation 3.8 with $n = 4$, $z_{i+1} - z_i = 0.6$ mm we calculated the slope for the upper edge (m_u, HP a - HP d) and the lower edge (m_l, HP d - HP g). We showed in measurements described above that the field in the center of the tape is proportional to the critical current. The slopes m_u and m_l can

41
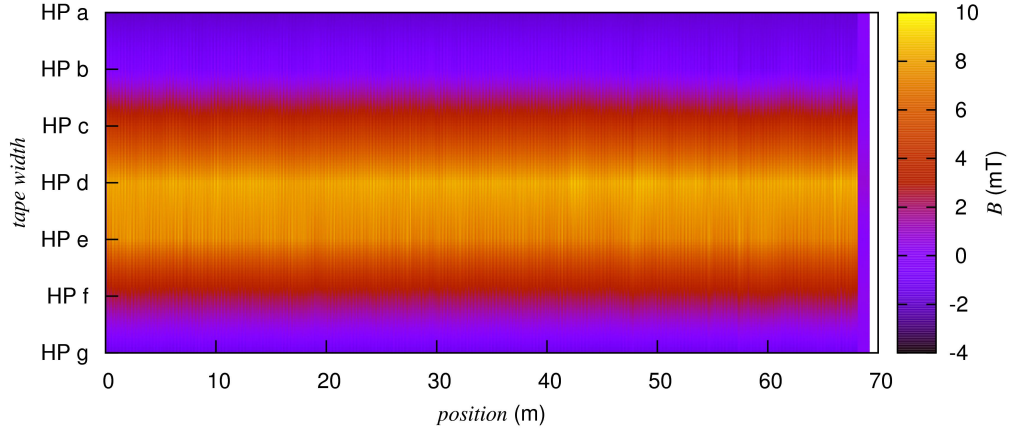
Figure 5.11: M3-998: Two dimensional map with coloring of the remanent field profile $B(x, z)$ (interpolated)

now be compared to the central field profile (fig. 5.12 (a)). It is obvious that the slopes are proportional to the remanent magnetization and therefore to the critical current profile. The mean values for m_u and m_l are $5.8\,\mathrm{mT/mm}$ and $5.5\,\mathrm{mT/mm}$, respectively. Hence, the expected field in the center is about $10\,\mathrm{mT}$, which matches with the results, given that Hall probe d is not perfectly centered.

To calculate the current flow, equation 3.12 was used, with $\Delta z = 0.6\,\mathrm{mm}$. The distance between tape and Hall probes Δy is crucial for this calculation. We calculated the current I with four different values for Δy: $0.5\,\mathrm{mm}$, $0.7\,\mathrm{mm}$, $1\,\mathrm{mm}$ and $1.2\,\mathrm{mm}$. The results for a short section of five meters are compared in figure 5.13. An actual distance between $1\,\mathrm{mm}$ and $1.2\,\mathrm{mm}$ is most likely. Positive currents flow in positive x-direction. In fig. 5.13 (a) and (b) the 28 cm variations are not apparent and do not strongly influence the maxima of the current flow. On the other hand they are significant in fig. 5.13 (c) and (d).

Figure 5.14 shows the field and current profiles at x=27.654 m, interpolated by cubic splines. To show a more exact Bean like behavior the resolution across the tape width, in z direction is still not sufficient. But two linear fits in figure 5.14 (a) (green lines) indicate this Bean shape and the position of the center of the tape as well (line-line intersection). When mounting the Hall probe array, the center of the tape was missed by about $0.2\,\mathrm{mm}$. Figure 5.14 (b) shows approximately the expected current distribution with currents flowing in positive and negative x-direction on the upper and lower edge, respectively. The current profile shown is calculated with $\Delta y = 1\,\mathrm{mm}$. It is clear that this profile is only a very simple approximation, neglecting any boundary effects. Since there are only seven measured points across the width, no corrections are made, e.g. that the currents vanish at the edges.

42
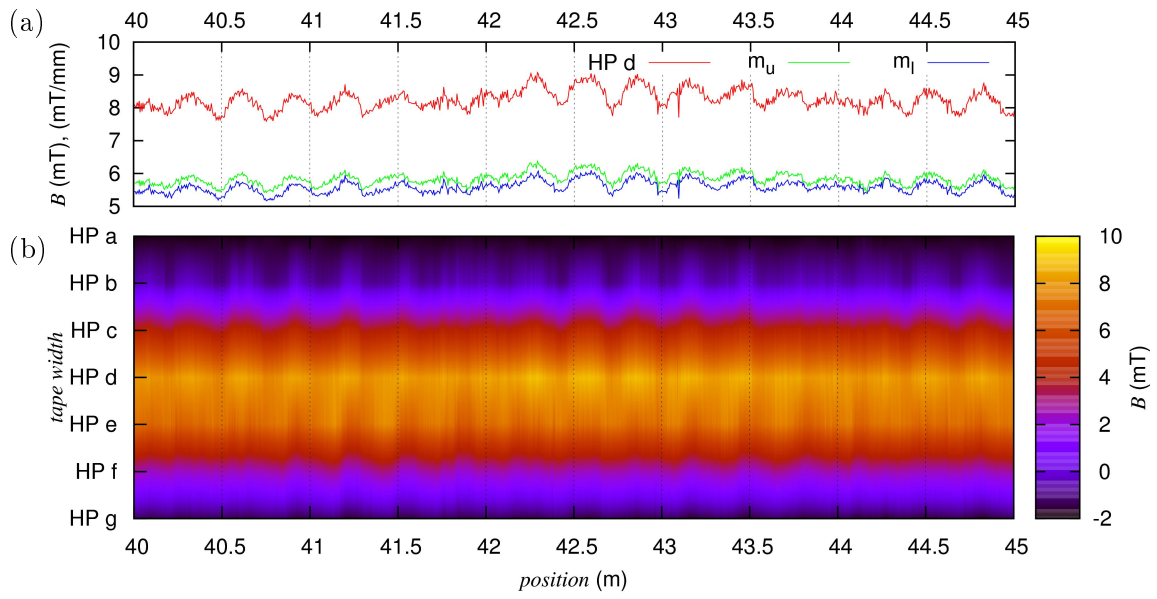
Figure 5.12: M3-998 in detail: (a) Field above the center of the tape (red curve) and the upper and lower slope (green and blue) in mT/mm; (b) 2D field map $B(x, z)$ (interpolated)
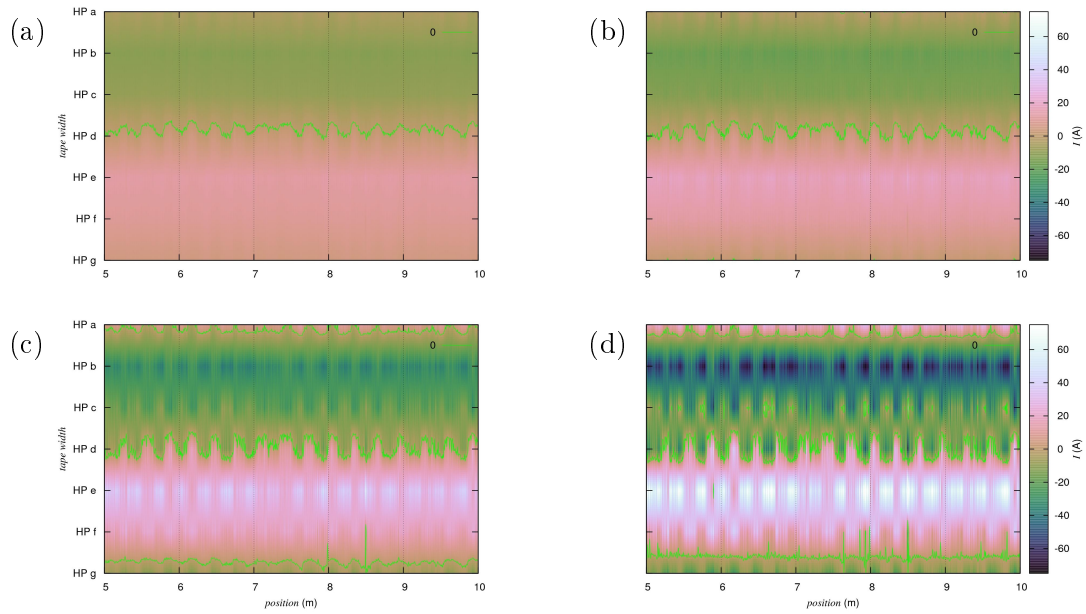
Figure 5.13: M3-998: 2D maps of current calculations $I(x, z)$ for different distances Δy between Hall probe surface and tape, (a) $\Delta y = 0.5$ mm, (b) $\Delta y = 0.7$ mm, (c) $\Delta y = 1$ mm, (d) $\Delta y = 1.2$ mm; the green lines indicate 0 A
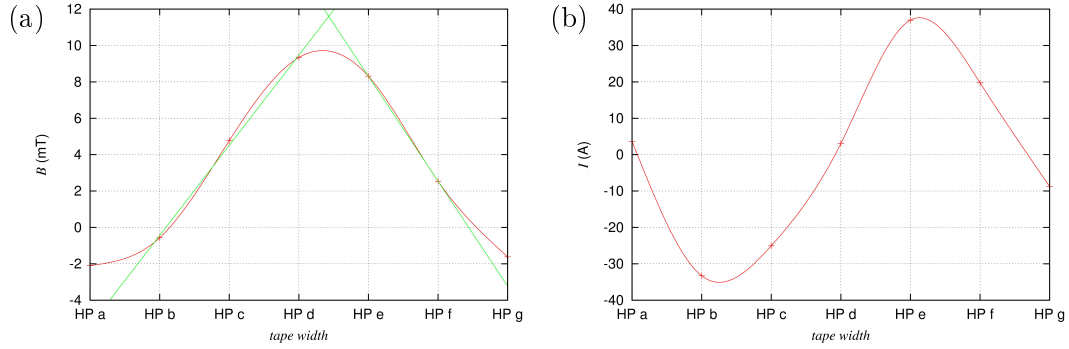
Figure 5.14: M3-998: Profile curves at position 27.7 m versus tape width, consecutive points are connected by natural cubic splines after rendering the data monotonic for (a) the measured field (b) the calculated current; the green lines in panel (a) are linear fits through points of HP b - HP d for the left side and HP e and HP f for the right side

5.5 Tape SP53

This tape is approximately 54 m long and was one of three tapes used to wind an all superconducting magnet that quenched at unexpectedly low currents. Quenches occur, if the field inside the magnet or the rate of change of the field is too large. Especially for coated conductors a local defect can be a source of quenches too. Therefore the tapes were unwound and analyzed with YatesStar. The other two tapes SP57 and SP59 are described later. The results for SP53 are shown in figure 5.15. The mean I_c of channel one, which was measured in the permanent magnet, is 37.4 A, with 0.032 as ratio of standard deviation to mean value. The local mean I_c changes with 1.37 mA/m. This is an extraordinary good result. It is probable, that the original tape orientation was lost and the end in fig. 5.15 was originally the tape beginning. The magnetic field produced by the electromagnet (1.09 T) was higher than that of the permanent magnet (0.53 T), therefore the in-field I_c values are lower. The mean I_c for channel two is 31.2 A, with a ratio of 0.034. The local average I_c decreases with 8.89 mA/m. The difference in the rate of decrease can be caused by a slightly increasing field of the electromagnet with time. Further the n-value, a dimensionless quantity, and the field of the central scan line are shown. The red, blue and magenta lines are linear fits through the measuring points of Channel 1, Channel 2 and the central Hall probe, respectively. While both I_c curves match each other, the Hall scan looses some details. Also the peak heights are less significant. On the other hand the drops are more intense and they correlate to drops in the I_c and/or the n-value profile. The average central field decreases with 1.76 µT/m, and over the full length it is 2.58 mT with a ratio (standard deviation divided by mean value) of 0.076. This low field might be caused by a dysfunction of the electromagnet and a larger distance between the sensors and the tape. The Hall probe array was fixed in between the electromagnet and the permanent magnet. The remanent magnetization measured with the Hall probes in the forward scan was induced by the electromagnet. A
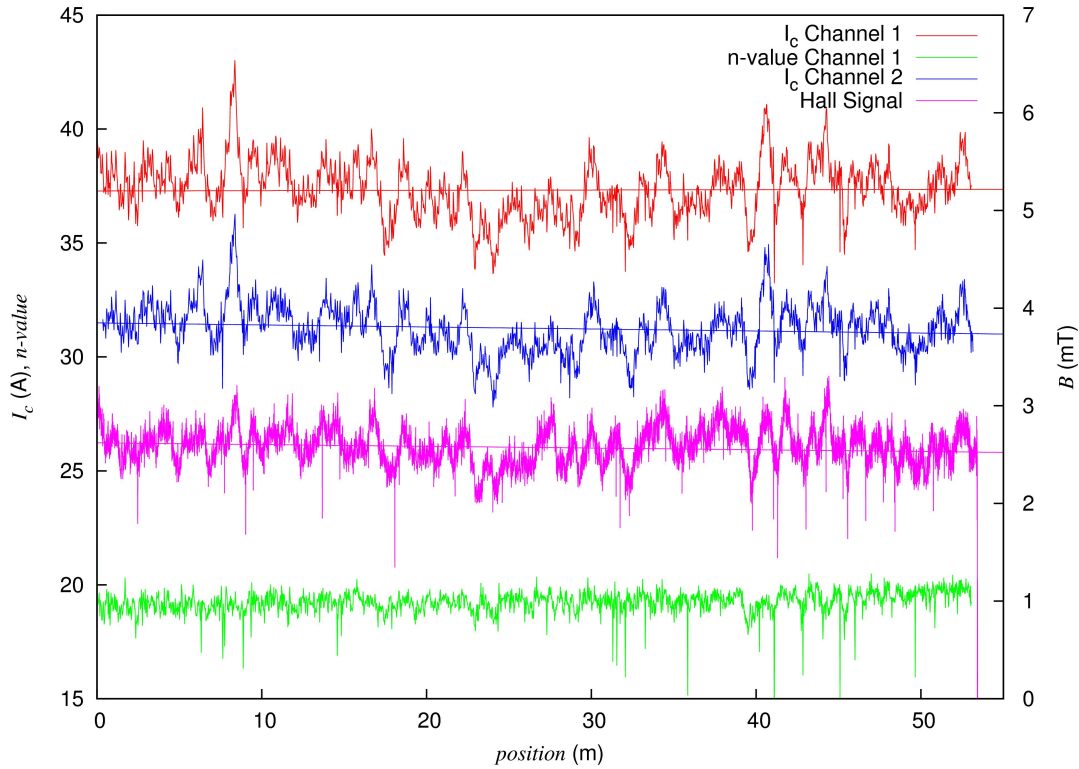
Figure 5.15: SP53: two simultaneous I_c measurements in different fields (red: $B_{max} = 0.53$ T, blue $B_{max} = 1.09$ T) and in situ magnetization measurement; the n-value shown is calculated from the current-voltage curve of channel one

repetition of the measurement backwards leads to an average field of 5.23 mT. The reason for this higher field remained unclear, but might be due to a smaller distance between the tape surface and the Hall probes.

A two dimensional map of the field $B(x, z)$ is shown in figure 5.16. We did not find any striking feature in this tape, which might be of concern in a magnet.

5.6 Tape SP57

Tape SP57 was the second tape investigated for major defects. Indeed, after 37 m, we found a huge drop to less than 50 % of the average I_c of this tape. Since the speed-up function was enabled, a rerun was necessary to resolve this defect in detail. The mean I_c values for Channel one and two are 40.2 A and 38.98 A, with standard deviation to mean value ratios of 0.044 and 0.047, respectively. The average decreases with 4.5 mA/m. The self field I_c of the bad spot is about 13.9 A, in field it further drops to 5.4 A. The whole measurement is shown in figure 5.17. The inset of this figure shows that all lines drop. The drops of the I_c measurements are wider. Usually the region in the center of the field
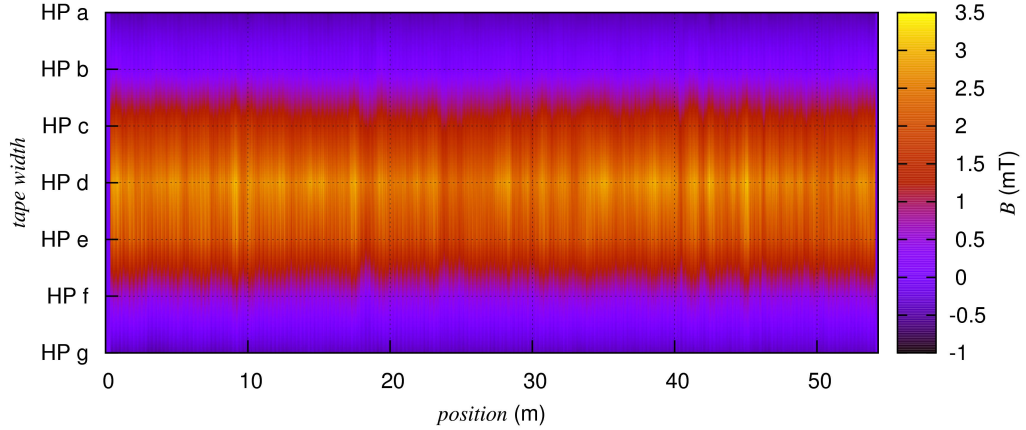
Figure 5.16: SP53: 2D map of the measured field $B(x,z)$ with seven Hall probes

B_{max} defines I_c, the distance between the voltage tabs can be neglected. In this case, the self field I_c of the damaged area is even worse than the average in-field I_c. Both I_c curves drop to the self field I_c of the bad spot as soon as it is in between the voltage tabs. When the defect moves into the center of the magnet the critical current drops further. The Hall probe signal even drops to 0 mT. Over the full length the 28 cm fluctuations are again clearly perceptible.

Figure 5.18 shows a two dimensional map of the remanent field $B(x,z)$ in an area close to the defect, measured with seven Hall probes. The green curve is the critical current I_c of channel one in arbitrary units. The bright areas of the map match the maxima in the current profile. Assuming a local maximum on the left side of defect (vertical blue line on the map) and according to the brighter area, the I_c fluctuations are easily comprehensible. This tape is termed a back slit, it is a side piece with only one cut surface (upper edge). The contours do not necessarily correlate exactly with the edges of the tape. The distance between Hall probes and tape might be too large to achieve more accurate results of the tape width. According to our measurements the width fluctuates by 3 % around the mean width. This result matches earlier measurements by Denis Markiewicz at the NHMFL. He measured the width variations and found that the width varies between 4 mm and 4.3 mm, ±3 % around the average of 4.15 mm.

For further investigations of this defect, a short sample of 20 cm was cut from the tape with the defect in the center. This short sample fits into the magnetoscan setup [42, 43] at the Atominstitut in Vienna, where it was analyzed again. The sample was fixed in a dewar immersed in liquid nitrogen. A magnet with a maximum field of 400 mT was moved along the surface of the tape for magnetization purposes. Then a single Hall probe, fixed to a computer controlled stepper motor, scanned the tape surface with a step size of 0.5 mm. The scan is plotted in figure 5.19. The width of the defect is 21 mm.
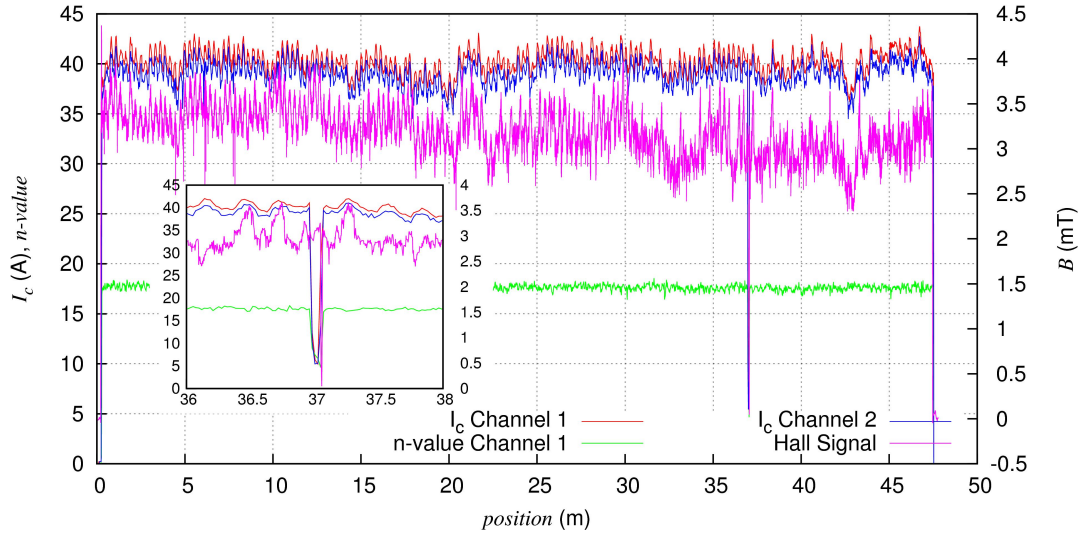
Figure 5.17: SP57: The results of the tape measurements; obvious defect at 37 m, observed in all scans (both I_c channels and Hall probes) and in the n-value evaluation; the inset shows the defect in detail, I_c drops to one eighth of the average

The apparently larger width (5-6 cm) of the defect in the I_c measurement is due to the finite distance between the voltage tabs as explained above.

These results prove the need for quality control of coated conductors for any applications and also prove the validity of our methods. We were able to find a major defect, which caused the quench of the magnet. Further, mechanical handling, like winding and unwinding the tape, does not necessarily harm the tape. We highly recommend to provide tapes to us before using them. Preliminary investigations should be established as a standard procedure at the NHMFL, which could save working hours and helium and prevent a possible damage of other tapes in case of a quench.

5.7 Tape SP59

With a length of 38 m, SP59 was the shortest tape of the three, which we investigated for damage. Hall probe and local transport current measurements were made, but we did not find any significant inhomogeneity. The results of these scans are shown in figure 5.20. This tape has a high average critical current of 43.4 A with a root mean square deviation of 3.29 A. The ratio of those two values is 0.079. The average I_c decreases with 243 mA/m, calculated over the full length of the tape. The average of the field in the center of the tape is 5.96 mT and its ratio with the standard deviation is 0.061. It decreases with 12 μT/m. In percent the critical current decreases with 0.6 %/m and the remanent field only with 0.2 %/m, indicated by the red and blue line in fig. 5.20. The difference in the rates of change leads to a non-constant calibration factor, which results in $c(x) = 7.7 - \frac{x}{50}$ A/mT
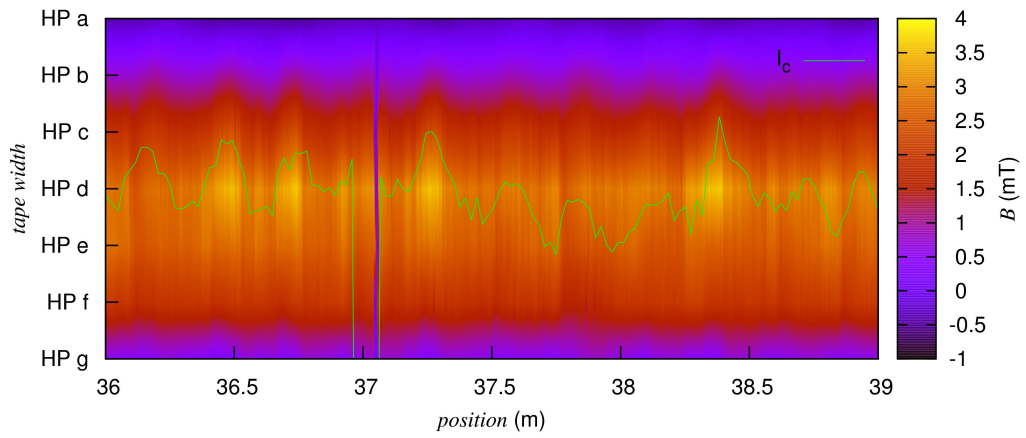
Figure 5.18: SP57: 2D map of the local remanent field $B(x, z)$ ± 1 m around the defect, the bright areas indicate a high critical current, which is confirmed by the green I_c curve
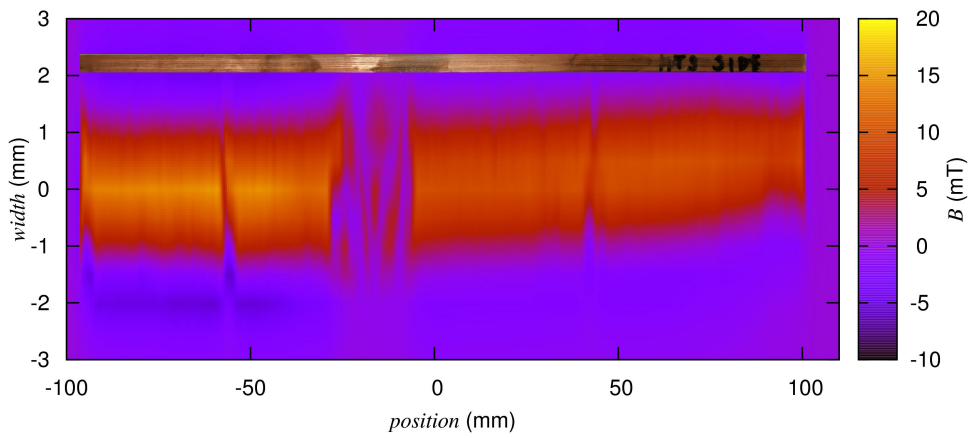
Figure 5.19: A short sample cut from the middle of SP57 was analyzed by a scanning Hall probe setup to achieve a higher resolution of the defect structure; the defect is about 21 mm wide; a picture of the sample is inserted, to demonstrate that no damages at the surface could possibly cause the disappearance of superconductivity (ratio of length to width is changed)
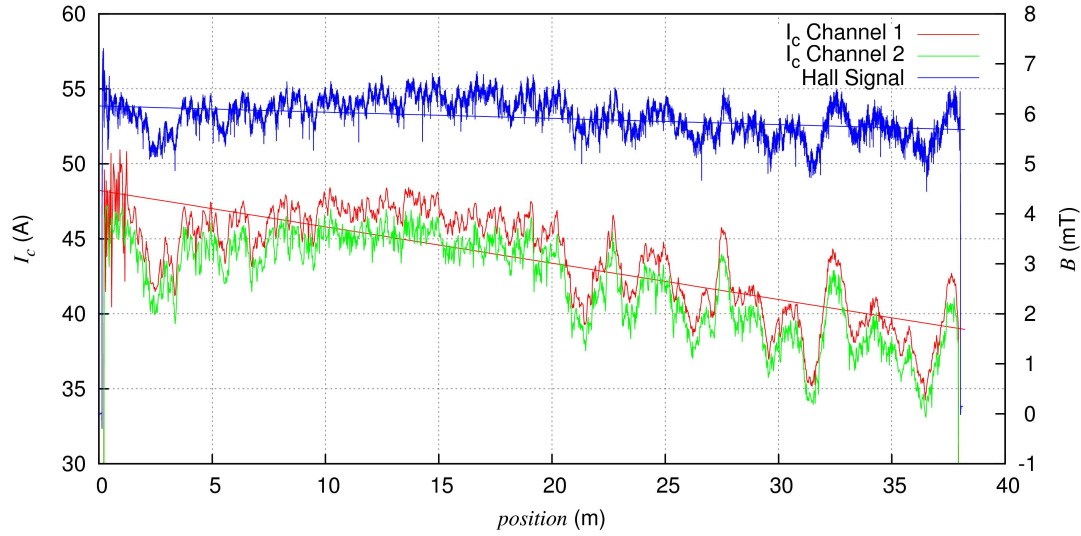
Figure 5.20: SP59: The critical current and remanent field profile over the full length of the tape, with linear fits for the I_c of channel one and the Hall signal (central Hall probe); short and long fluctuations were observed; the variations in the first meter of the red line do not correlate to real I_c variations

with x in meters. The width fluctuations were less significant than in other measurements. Several fluctuations superpose. Especially after 20 m the behavior of the critical current changes dramatically. Those long fluctuations seriously worsen the result of this tape. It remained unclear, whether chemical or mechanical modifications in the production during the manufacturing process caused these fluctuations. The high amplitude of channel one in the first meter might be caused by a bad contact. Similar signal variations were not observed in the signal of channel two nor in the Hall measurement. Figure 5.21 shows a histogram of the distribution of the currents. The inset takes only the first 20 m into account. A Gaussian function $g(x) = a \cdot \exp(-\frac{(x-b)^2}{c^2})$ is fitted to the data via the fit parameters a, b and c. For the first half of the tape (inset) a Gaussian distribution approximately matches the current distribution while the full tape cannot be described by a Gaussian function. It is not clear, which processes are responsible for these fluctuations leading to the present non-normal distribution.

5.8 Tape Collection (SP60-SP64)

The tape collection is a composition of ten short tape samples, which were soldered together. Each sample is about 60 cm long and the whole collection is 6 m long. The samples were cut from both ends of the tapes SP60, SP61, SP62, SP63 and SP64, respectively. The terms inner (i) and outer (o) end relate to the orientation of the tapes in a spool, which was built with those tapes. Before the short samples got coupled together, their self field critical current $I_{c,sf}$ at 77 K was measured by Dr. Dmytro Abraimov at the
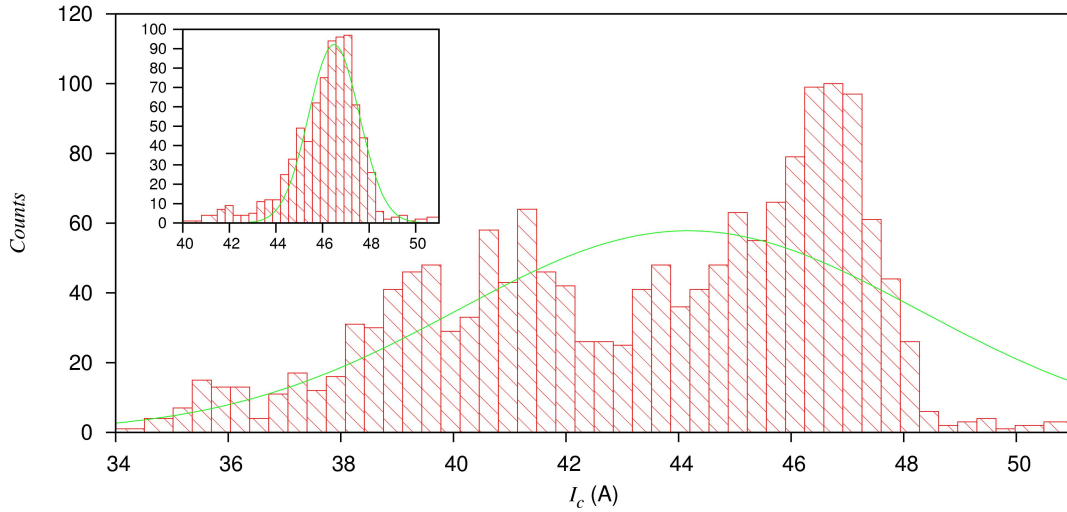
Figure 5.21: SP59: Distribution of critical currents over the full length (inset: only over the first 20 m) of the coated conductor; a Gaussian distribution is fitted to the data

NHMFL. In YatesStar we analyzed the in-field I_c and remanent field. The results are shown in figure 5.22. There are three y-axes. The very left shows the range of the self field measurement which are depicted as red boxes, followed by the y-axis for the in-field results. The scale for the magnetic measurement is on the right side of the plot. The self field I_c was measured in two short samples, each 50 mm long, and, therefore is defined by the minimum current. The high green peaks of the signal of the central Hall probe (HP d) correspond to the coupling joints between the tapes. The Hall signal $B(x)$ and the self field critical current $I_{c,sf}$ correlate very well, which is obvious in samples SP60i and SP61o, with exception of sample SP64i and SP64o. The results are listed in table 5.2, whereby $\bar{I}_c(x)$ and $\bar{B}(x)$ are the mean values of the YatesStar I_c and magnetization measurements. The results are displayed once more in figure 5.23, where the self field critical current is plotted versus the in-field critical current. The inner ends are indicated by red points, the outer by green ones. There is no simple correlation valid for all tapes. If the tapes are viewed individually, a higher self field I_c correlates with a higher in-field current. Lines are drawn to guide the eye and make this correlation clearer. The ratio $I_{c,sf}/I_c$ varies between 2.29 (SP62i,SP64i&o) and 2.72 (SP60i). According to the information we have, all tapes had originally a length of 110 m. This implies that the in-field I_c changes between $9\,\mathrm{mAm}^{-1}$ (SP62) and $80\,\mathrm{mAm}^{-1}$ (SP60) and the self field critical current changes between $22\,\mathrm{mAm}^{-1}$ (SP61) and $66\,\mathrm{mAm}^{-1}$ (SP63).
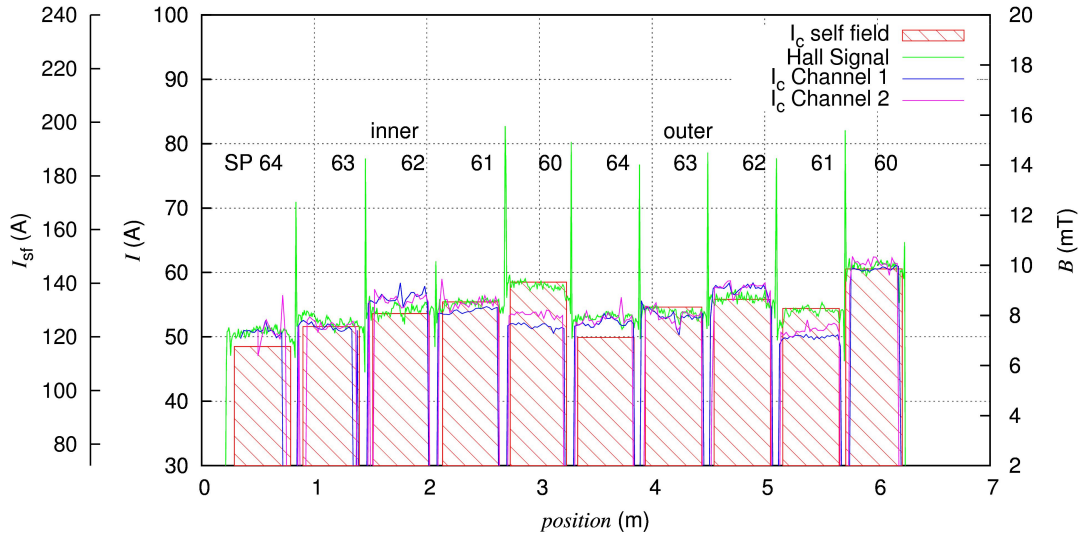
Figure 5.22: Summery of three different measurements on the 10 short samples of the tape collection: the red boxes are the results of the self field measurements, the green curve is the reel-to-reel Hall probe result and the blue and magenta profiles are the in-field I_c values measured with YatesStar
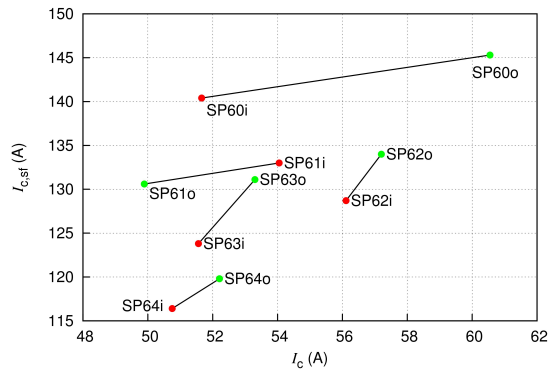
Figure 5.23: $I_{c,sf}$ versus I_c. No simple correlation is observed, which is valid for all tapes; only for individual tapes do higher $I_{c,sf}$ values correlate with higher in-field currents

51

SP	64i	63i	62i	61i	60i	64o	63o	62o	61o	60o
$\bar{I}_{\mathrm{c}}(x)$ (A)	50.8	51.6	56.1	54.1	51.7	52.2	53.3	57.2	49.9	60.6
$\bar{B}(x)$ (mT)	7.3	7.7	8.2	8.4	9.2	7.9	8.1	8.7	8.1	9.9
$I_{\mathrm{c,sf}}$ (A)	116.4	123.8	128.7	133	140.4	119.8	131.1	134	130.6	145.3

Table 5.2: Results of different measurements of the tape collection

5.9 Tape SP41 at 4.2 K

During one of the first tests in liquid helium with the newly developed extension for YS*, the first 10 m of the tape got destroyed, when it lost tension and got caught between a pulley and the mounting. Subsequently added stabilizers ensure better measurements. For our test procedures the destroyed areas in the tape were useful allowing us to adjust the position of several different runs. Due to the new defects it was necessary to repeat the I_{c} and magnetization measurements in liquid nitrogen. Figure 5.24 compares unique reel-to-reel results at 4.2 K with the new transport current and magnetization measurements at 77 K. The remanent magnetization was produced by a magnetic field of 0.5 T. The remanent field at 4.2 K exceeds the magnetization at 77 K by a factor of 15. The self field critical currents at low temperatures are far beyond 1 kA. Correlations between the I_{c} curve and the green magnetization profile are obvious. The low temperature Hall probe measurement correlates to the critical current as well.

The defects, which had already been observed in earlier magnetization measurements at 77 K (figure 5.8 on page 39), were measured again. In the first measurement at liquid nitrogen the Hall voltage at the defect at ≈ 23 m drops to 60% of the mean value. In the second run it drops to zero. While the I_{c} of the rest of the tape was not degraded by mechanical handling, the defect itself got worse. Both, transport and magnetization method indicate, that the superconducting layer got completely destroyed in this section. Further investigations on the evolution of defects is important for users, because applications require mechanical handling.

5.10 Tape Collection (SP60-SP64) at 4.2 K

The collection of ten short samples was also measured in liquid helium. The results are shown in figure 5.25. The external field was set to 0.5 T, which did not exceed $2B^*$. Hence the state of full remanent magnetization was not reached. The signal of the center Hall probe (HP d) does not necessarily correlate to I_{c}. This situation might be more complex, because two local maxima contribute to the signal in the center. The left inset shows the calculated field gradients. m_{u} is calculated over HP a - HP c, and m_{l} is calculated over HP e - HP g. The results agree with the average gradients of each sample. A high gradient correlates with a high critical current in self field. The results of SP60 at 4.2 K match the results at 77 K. The right inset shows the field profile of three selected samples. It is obvious that full magnetization is not reached. A linear extrapolation yields a field
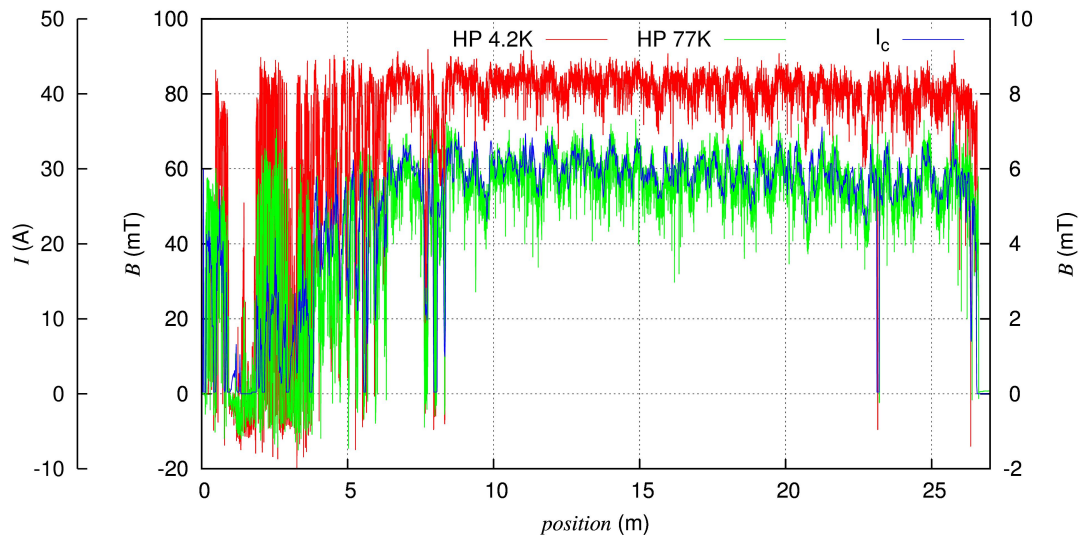
Figure 5.24: Comparison of reel-to-reel measurements at 4.2 K and 77 K; the very left scale corresponds to the I_c measurement at 77 K and the right scale to the Hall probe measurement at 77 K. The second scale on the left refers to the Hall probe measurement at 4.2 K.

of 120 mT to 140 mT in the center of the tape. Spikes already observed in liquid nitrogen are again seen in helium (e.g. SP62i).
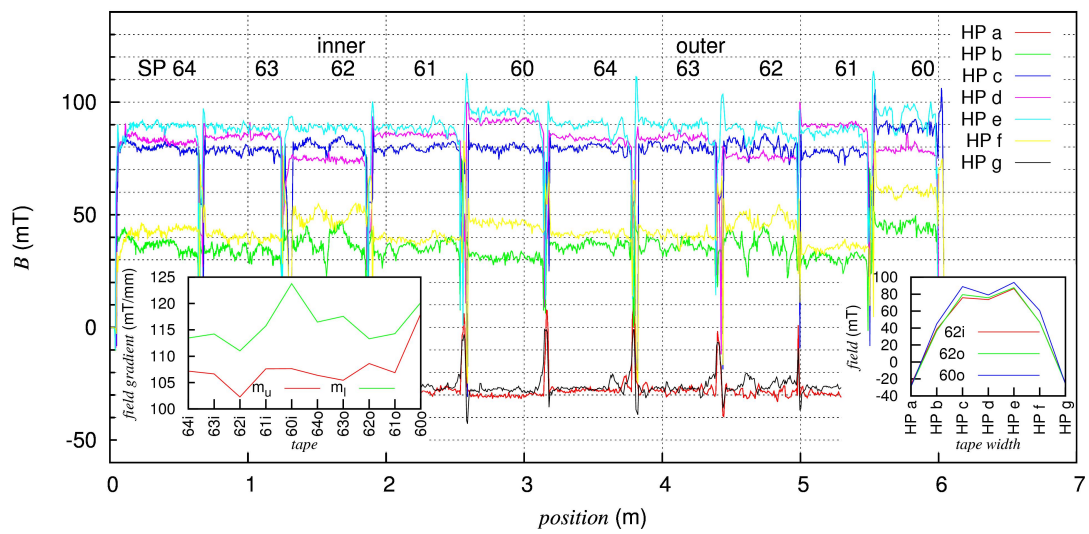
Figure 5.25: Tape collection: remanent field of 10 short samples at 4.2 K, magnetized in 0.5 T; the tapes were not fully magnetized; the left inset shows the average field gradient of each sample at both edges; the right inset shows the field profile over the tape width for three samples

6 Conclusions and Outlook

The tapes investigated in this study are listed in table 6.1 with a short summery of the numerical results. The main results of this work were

- the development and improvement of methods for the characterization of REBCO superconductors for power generation/transmission as well as scientific and medical applications,

- quality testing for all superconducting high field magnets currently under construction at the NHMFL,

- detailed comparison of two independent characterization methods and validation of continuous magnetization measurements to find inhomogeneities in coated conductors with high speed and high resolution in a non-destructive manner,

- discovery of problems in the commercial manufacturing process of coated conductors causing variations in their physical properties and therefore in the quality of the tape (width variations, I_c fluctuations with different magnitudes and periodicities, changes of the self field $I_{c,sf}$ to the in-field I_c ratio, Gaussian and non-Gaussian current distributions),

- pioneer development of reel-to-reel magnetization measurements in liquid helium to assess the critical current and find inhomogeneities and

- first comparisons of $4.2\,\mathrm{K}$ reel-to-reel magnetization measurements with $77\,\mathrm{K}$ measurements.

Parts of this work were presented in three conference contributions at EUCAS in September 2013 and a publication is currently in preparation.

The ASC will continue the research on the analysis of coated conductors. Therefore new Hall probe arrays, the MULTI-7U models from AREPOC s.r.o, were purchased. Those Hall probes are designed to operate at very low temperatures and fields of up to $5\,\mathrm{T}$. The aim is to compare very cheap Hall probes, which are used in this work, with expensive models to find possibilities to further improve the setup. For the tape analysis at $77\,\mathrm{K}$ there are plans to apply a small AC voltage on the conductor, to make small defects in the center of the tape visible by shifting the region where no currents are flowing. Furthermore more measurements at $4.2\,\mathrm{K}$ need to be done, especially in-field measurements at different fields.

SuperPower Label	NHMFL in House "SP" Label	Project	Length (m)	$\bar{I}_c$ (A)	$R_{\bar{I}_c}$	R_B
M3-747-2-BS		Platypus I	116	48.8	46	64
M4-52-2-FS		Platypus I	110	45.4	67	109
M3-891-1 FS	SP41	YS* tests	26	29.6	75	43
M3-998-2 MS 1224.6-1324.6		Platypus I	69			33
M3-842-1 MS	SP53	32 T Project	54	37.4	32	76
M4-52-2 BS	SP57	32 T Project	48	40.2	44	87
M4-52-2 FS	SP59	32 T Project	38	43.4	79	61
M3-1029-1 MS 979-1089.7	SP60	32 T Project	1.2	56.2		
M3-1038-2 BS 148.44-258.44	SP61	32 T Project	1.2	52		
M3-1038-2 FS 423.44-533.44	SP62	32 T Project	1.2	56.7		
M3-1038-2 BS 309-419	SP63	32 T Project	1.2	52.5		
M3-1038-2 BS 419-529	SP64	32 T Project	1.2	51.5		

Table 6.1: Listing of tapes and results of 77 K measurements; the third column lists the project for which the tape is used; the fifth column gives information about the mean critical current $\bar{I}_c$ (in-field) over the full length of the conductor; $R_{\bar{I}_c}$ and R_B are the ratios of standard deviation to mean value multiplied by 1000 for the I_c and Hall probe measurements

Bibliography

[1] J. Y. Coulter, T. G. Holesinger, J. A. Kennison, J. O. Willis, and M. W. Rupich. Nondestructive Investigation of Position Dependent I_c Variations in Multi-Meter Coated Conductors. *IEEE Trans. Appl. Supercond.*, 19(3):3609 –3613, 2009.

[2] J. Y. Coulter, J. Haenisch, J. O. Willis, L. Civale, and W. K. Pierce. Position and Magnetic Field Angle Dependent I_c for Long-Length Coated Conductors. *IEEE Trans. Appl. Supercond.*, 17(2):3394 – 3397, 2007.

[3] J. O. Willis, J. Y. Coulter, and M. W. Rupich. n-Value Analysis of Position-Dependent Property Variability in Long-Length Coated Conductors. *IEEE Trans. Appl. Supercond.*, 21(3):2988 – 2991, 2011.

[4] H. W. Weijers, W. D. Markiewicz, and D. C. Larbalestier. Development of a 32 T All-Superconducting Magnet System using $YBa_2Cu_3O_{7-x}$ Coated Conductors. Technical report, National High Magnetic Field Laboratory, 2012.

[5] K. P. Thaku, R. A. Badcock, N. J. Long, and K. A. Hamilton. Analysis of Remnant Field Detected by Hall Sensors. *Proc. IEEE Sensors Conf.*, pages 244 – 247, 2009.

[6] M. Inoue, K. Abiru, Y. Honda, T. Kiss, Y. Iijima, K. Kakimoto, T. Saitoh, K. Nakao, and Yuh Shiohara. Observation of Current Distribution in High Tc Superconducting Tape Using Scanning Hall-Probe Microscope. *IEEE Trans. Appl. Supercond.*, 19(3): 2847 – 2850, 2009.

[7] S. Furtner, R. Nemetschek, R. Semerad, G. Sigl, and W. Prusseit. Reel-to-reel critical current measurement of coated conductors. *Supercond. Sci. Technol.*, 17: S281, 2004.

[8] G. Grimaldi, M. Bauer, and H. Kinder. Continuous reel-to-reel measurement of critical currents of coated conductors. *Appl. Phys. Lett.*, 79(26):4390 – 4392, 2001.

[9] J. Jaroszynski, D. Abraimov, V. Braccini, M. Santos, A. Xu, A. Polyanskii, Y. Coulter, J. W. Sinclair, H. Weijers, W. D. Markiewicz, and D.C. Larbalestier. Testing procedures on IBAD-MOCVD coated conductors for thier use at high magnetic field and low temperature in magnet applications. to be published.

[10] V. Braccini, A. Xu, J. Jaroszynski, Y. Xin, D. C. Larbalestier, Y. Chen, G. Carota, J. Dackow, I. Kesgin, Y. Yao, A. Guevara, T. Shi, and V. Selvamanickam. Properties of recent IBAD–MOCVD coated conductors relevant to their high field, low temperature magnet use. *Supercond. Sci. Technol.*, 24:035001, 2011.

[11] A. Xu, V. Braccini, J. Jaroszynski, Y. Xin, and D. C. Larbalestier. Role of weak uncorrelated pinning introduced by $BaZrO_3$ nanorods at low-temperature in $(Y,Gd)Ba_2Cu_3O_x$ thin films. *Phys. Rev. B*, 86:115416, 2012.

[12] W. Meissner and R. Ochsenfeld. Ein neuer Effekt bei Eintritt der Supraleitfähigkeit. *Naturwissenschaften*, 21(44):787 − 788, 1933.

[13] W. Buckel and R. Kleiner. *Superconductivity: fundamentals and applications*. WILEY-VCH Verlag, 2004.

[14] K. H. Bennemann, J. B. Ketterson, and L. Pitaevskii. *Superconductivity Conventional and Unconventional Superconductors*. Springer-Verlag, 2 edition, 2008. ISBN 978-3-540-73252-5.

[15] H. W. Weber and O. Hittmair. *Supraleitung*. Verlag Karl Thiemig, 1979. ISBN 3-521-06113-2.

[16] A. A. Abrikosov. On the Magnetic Properties of Superconductors of the Second Group. *Sov. Phys. JETP*, 5(6):1442, 1957.

[17] J. G. Bednorz and K. A. Müller. Possible high T_c superconductivity in the Ba-La-Cu-O system. *Zeitschrift für Physik B*, 64:189 − 193, 1986.

[18] M. K. Wu, J. R. Ashburn, C. J. Torng, P. H. Hor, R. L. Meng, L. Gao, Z. J. Huang, Y. Q. Wang, and C. W. Chu. Superconductivity at 93 K in a Mixed-Phase Y-Ba-Cu-O Compound System at Ambient Pressure. *Phys. Rev. Letters*, 58(9):908, 1987.

[19] A. Schilling, M. Cantoni, J. D. Guo, and H. R. Ott. Superconductivity above 130 K in the Hg-Ba-Ca-Cu-O system. *Nature*, 363:56 − 58, 1993.

[20] C. W. Chu, L. Gao, F. Chen, Z. J. Huang, R. L. Meng, and Y. Y. Xue. Superconductivity above 150 K in $HgBa_2Ca_2Cu_3O_{8+\delta}$ at high pressures. *Letters to Nature*, 365:323, 1993.

[21] L. Gao, Y. Y. Xue, F. Chen, Q. Xiong, R. L. Meng, D. Ramirez, and C. W. Chu. Superconductivity up to 164 K in $HgBa_2Ca_{m-1}Cu_mO_{2m+2+\delta}$ (m=1, 2, and 3) under quasihydrostatic pressures. *Phys. Rev. B*, 50(6):4260, 1994.

[22] J. Bardeen, L. N. Cooper, and J. R. Schrieffer. Microscopic Theory of Superconductivity. *Phys. Rev.*, 106:162 − 164, 1957.

[23] S. L. Bud'ko, G. Lapertot, C. Petrovic, C. E. Cunningham, N. Anderson, and P. C. Canfield. Boron Isotope Effect in Superconducting MgB_2. *Phys. Rev. Letters*, 86: 1877 − 1880, 2001.

[24] Y. Kamihara, H. Hiramatsu, M. Hirano, R. Kawamura, H. Yanagi, T. Kamiya, and H. Hosono. Iron-Based Layered Superconductor: LaOFeP. *J. Am. Chem. Soc.*, 128: 10012 − 10013, 2006.

[25] Y. Kamihara, T. Watanabe, M. Hirano, and H. Hosono. Iron-Based Layered Superconductor La[O$_{1-x}$F$_x$]FeAs (x = 0.05-0.12) with T_c = 26 K. *J. Am. Chem. Soc.*, 130:3296 − 3297, 2008.

[26] US Department of Energy. Timeline of discoveries of superconducting materials. URL `http://www.ccas-web.org/superconductivity`.

[27] C. P. Bean. Magnetization of Hard Superconductors. *Phys. Rev. Letters*, 8(6):250 − 253, 1962.

[28] C. P. Bean. Magnetization of High-Field Superconductors. *Rev. Mod. Phys.*, 36:31 − 39, 1964.

[29] Y. B. Kim, C. F. Hempstead, and A. R. Strnad. Magnetization and Critical Supercurrents. *Phys. Rev.*, 129(2):528 − 536, 1963.

[30] M. Eisterer. Hochtemperatursupraleitung, 2012. Lecture notes.

[31] H. Hilgenkamp and J. Mannhart. Grain boundaries in high-T_c superconductors. *Rev. Mod. Phys.*, 74:485 − 549, 2002.

[32] J. D. Jorgensen, B. W. Veal, A. P. Paulikas, L. J. Nowicki, G. W. Crabtree, H. Claus, and W. K. Kwok. Structural properties of oxygen-deficient YBa$_2$Cu$_3$O$_{7-\delta}$. *Phys. Rev. B*, 41:1863 − 1877, 1990.

[33] J. B. Ketterson and S. N. Song. *Superconductivity*. Cambridge University Press, 1999. ISBN 0-521-56295-3.

[34] A. Damascelli, Z.-X. Shen, and Z. Hussain. Angle-resolved photoemission spectroscopy of the cuprate superconductors. *Rev. Mod. Phys.*, 75(2):473, 2003.

[35] J. W. Farmer, D. L. Cowan, and M. Kornecki. Collective pinning model of the mixed state in YBa$_2$Cu$_3$O$_{7-\delta}$: Critical currents and flux creep. *Phys. Rev. B*, 77(5): 054514, 2008.

[36] Aixia Xu. *Flux Pinning Study of ReBa$_2$Cu$_3$O$_{7-\delta}$ Coated Conductors for High Field Magnet Applications*. PhD thesis, Florida State University, FAMU-FSU College of Engineering, 2012.

[37] M. V. Feigel'man and V. M. Vinokur. Thermal fluctuations of vortex lines, pinning, and creep in high-t$_c$ superconductors. *Phys. Rev. B*, 41:8986, 1990.

[38] V. L. Pokrovskii. Magnitude and anisotropy of the penetration depth in high-temperature superconductors. *Pis'ma Zh. Eksp. Teor. Fiz.*, 47(10):539 − 541, 1988.

[39] R. Bhattacharya and M. P. Paranthaman. *High Temperature Superconductors*. WILEY-VCH Verlag GmbH & Co. KGaA, 2010. ISBN 978-3-527-40827-6.

[40] E. H. Hall. On a new Action of the Magnet on Electric Currents. *Amer. J. Math.*, 2:287 − 292, 1879.

[41] Georg-August Universität Göttingen. Die Hall-Sonde. URL https://lp.uni-goettingen.de/get/image/4581.

[42] M. Eisterer, S. Haindl, T. Wojcik, and H. W. Weber. "Magnetoscan": A Modified Hall Probe Scanning Technique for the Detection of Inhomogeneities in Bulk High Temperature Superconductors. *Supercond. Sci. Technol.*, 16(11):1282, 2003.

[43] S. Haindl. A novel magnetoscan design. *Supercond. Sci. Technol.*, 18(11):1483, 2005.

[44] J. W. Sinclair, J. Jaroszynski, A. Stangl, X. Hu, M. Santos, Y. Coulter, D. Abraimov, H. Weijers, W. D. Markiewicz, and D. C. Larbalestier. High current homogeneity in commercial REBCO coated conductors. to be published.

[45] M. Zehetmayer, R. Fuger, M. Eisterer, F. Hengstberger, and H. W. Weber. Assessment of the local supercurrent densities in long superconducting coated conductors. *Appl. Phys. Lett.*, 90(3):032506, 2007.

[46] E. H. Brandt and M. Indenbom. Type-II-superconductor strip with current in a perpendicular magnetic field. *Phys. Rev. B*, 48(17):12893 – 12906, 1993.

[47] *SuperPower 2G HTS Wire Specifications*. SuperPower Inc., 2011.

List of Figures

63

List of Tables